Acoustic In-duct Characterization of Fluid Machines with Applications to Medium Speed IC-engines

ANTTI HYNNINEN

Doctoral Thesis
Stockholm, Sweden 2015

TRITA-AVE 2015:86
ISSN 1651-7660
ISBN 978-91-7595-765-4

KTH The Marcus Wallenberg Laboratory
for Sound and Vibration Research
SE-100 44 Stockholm, SWEDEN

Akademisk avhandling som med tillstånd av Kunglika Tekniska Högskolan i Stockholm framlägges till offentlig granskning för avläggande av teknologie doktorsexamen torsdagen den 10:e december 2015 klockan 10:00 i Sal F3, Lindstedtsvägen 26, Kungliga Tekniska Högskolan, Stockholm.

Tryck: Universitetsservice US AB

Abstract

The unwanted sound, noise, can lead to health problems, e.g. hearing loss and stress-related problems. A pre-knowledge of noise generation by machines is of great importance due to the ever-shorter product development cycles and stricter noise legislation. The noise from a machine radiates to the environment indirectly via the foundation structure and directly via the surrounding fluid. A fluid machine converts the energy from the fluid into mechanical energy or vice versa. Examples of the fluid machines are internal combustion engines (IC-engines), pumps, compressors, and fans. Predicting and controlling noise from a fluid machine requires a model of the noise sources themselves, i.e. acoustic source data. In the duct systems connected to the fluid machines, the acoustic source interacts strongly with the system boundaries, and the source characteristics must be described using in-duct methods.

Above a certain frequency, i.e. first non-plane wave mode cut-on frequency, the sound pressure varies over the duct cross-section and non-plane waves are introduced. For a number of applications, the plane wave range dominates and the non-plane waves can be neglected. But for machines connected to large ducts, the non-plane wave range is also important. In the plane wave range, one-dimensional process simulation software can be used to predict, e.g. for IC-engines, the acoustic in-duct source characteristics. The high frequency phenomena with non-plane waves are so complicated, however, that it is practically impossible to simulate them accurately. Thus, in order to develop methods to estimate the sound produced, experimental studies are also essential.

This thesis investigates the acoustic in-duct source characterization of fluid machines with applications to exhaust noise from medium speed IC-engines. This corresponds to large engines used for power plants or on ships, for which the non-plane wave range also becomes important. The plane wave source characterization methods are extended into the higher frequency range with non-plane waves. In addition, methods to determine non-plane wave range damping for typical elements in exhaust systems, e.g. after-treatment devices, are discussed.

Sammanfattning

Oönskat ljud, buller, kan leda till hälsoproblem, t.ex. hörselnedsättning och stressrelaterade problem. Det är mycket viktigt med förkunskap om maskiners bullergenerering på grund av allt kortare produktutvecklingscykler och strängare bullerlagstiftning. Bullret från en maskin sprids till omgivningen indirekt via fundamentets struktur och direkt via omgivande fluid. En fluidkemaskin omvandlar fluidens energi till mekanisk energi, eller vice versa. Exempel på fluidmaskiner är förbränningsmotorer, pumpar, kompressorer och fläktar. För att förutsäga och kontrollera buller från en fluidmaskin krävs det en modell av själva bullerkällorna, alltså uppgifter om akustiska källor. I kanalsystemen som ansluts till fluidmaskinerna samverkar den akustiska källan starkt med systemets gränser och källans egenskaper måste beskrivas genom mätning inuti kanalen.

Över en viss frekvens, d.v.s. första tillslagsfrekvensen för icke-plana vågor, varierar ljudtrycket över kanalens tvärsnitt och icke-plana vågor införs. För ett antal tillämpningar dominerar området med plana vågor och de icke-plana vågorna kan ignoreras. Men för maskiner som ansluts till stora kanaler är också det icke-plana vågområdet viktigt. I det plana vågområdet kan endimensionell processimuleringsprogramvara användas för att förutsäga, t.ex. för förbränningsmotorer, egenskaperna för akustiska källor inuti kanalen. Fenomenen med höga frekvenser och icke-plana vågor är emellertid så komplicerade att det är praktiskt taget omöjligt att simulera dem med precision. Därför är också experimentella studier avgörande för att utveckla metoder för uppskattning av det ljud som uppstår.

Denna avhandling undersöker karakterisering, utförd inuti kanalen, av akustiska källor för fluidmaskiner med tillämpningar för avgasljud från medelhastighetsförbränningsmotorer. Detta motsvarar stora motorer som används för kraftverk eller på fartyg, för vilka de icke-plana vågornas område också blir viktigt. Metoderna för karakterisering av de plana vågornas källor utvidgas in i det högre frekvensområdet med icke-plana vågor. Dessutom avhandlas metoder för att i de icke-plana vågornas område fastställa dämpning för typiska element i avgassystem, t.ex. efterbehandlingsenheter.

Doctoral thesis

This thesis consists of the following papers:

Paper I
A. Hynninen, R. Turunen, M. Åbom, and H. Bodén. Acoustic source data for medium speed IC-engines. *Journal of Vibration and Acoustics*, **134**:051008, 2012, doi:10.1115/1.4006415.

Paper II
A. Hynninen, and M. Åbom. Procedure to estimate the in-duct sound power in the high frequency range with non-plane waves. *ASME 2012 Noise Control and Acoustics Division Conference at Inter-Noise 2012, New York City, New York, USA*, pp. 181-191, 2012, doi:10.1115/NCAD2012-0531.

Paper III
A. Hynninen, and M. Åbom. Acoustic source characterization for prediction of medium speed diesel engine exhaust noise. *Journal of Vibration and Acoustics*, **136**:021008, 2014, doi:10.1115/1.4026138.

Paper IV
A. Hynninen, and M. Åbom. Determination of in-duct sound power beyond the plane wave range using wall-mounted microphones. *Applied Acoustics*, **99**:24–30, 2015, doi:10.1016/j.apacoust.2015.05.003.

Paper V
A. Hynninen, and M. Åbom. Acoustic simulation of medium speed IC-engine exhaust gas after treatment devices with substrate. *SAE Technical Paper 2014-01-2057*, 2014, doi:10.4271/2014-01-2057.

Paper VI
A. Hynninen, and M. Åbom. Simulation of the particle oxidation catalyst POC® acoustics. *Noise Control Engineering Journal*, **62**(5):368–374, September 2014, doi:10.3397/1/376236.

Division of work between the authors

Paper I. Hynninen arranged the measurements, simulated the exhaust noise acoustics and wrote the paper, Turunen constructed the engine performance simulation model. The paper was supervised by Åbom and Bodén.

Paper II. Hynninen arranged the experiments, performed the analysis and wrote the paper. The paper was supervised by Åbom.

Paper III. Hynninen performed the analysis and wrote the paper based on the theory developed by Hynninen and Åbom. The paper was supervised by Åbom.

Paper IV. Hynninen performed the simulations and wrote the paper based on the theory developed by Hynninen and Åbom. The paper was supervised by Åbom.

Paper V. Hynninen performed the simulations and wrote the paper based on the methods developed by Hynninen and Åbom. The paper was supervised by Åbom.

Paper VI. Hynninen arranged the measurements, performed the analysis, constructed the simulation model and wrote the paper based on the methods developed by Hynninen and Åbom. The paper was supervised by Åbom.

Acknowledgements

The research in this thesis has been carried out at VTT Technical Research Centre of Finland, in cooperation with the Competence Center for Gas Exchange (CCGEx) at the Marcus Wallenberg Laboratory (MWL), Royal Institute of Technology (KTH), Stockholm, Sweden. The work was also supported by Wärtsilä Finland Ltd, Power Plants.

My supervisors Mats Åbom and Hans Bodén are greatly acknowledged.

Contents

Part I

Overview and Summary

Chapter 1

Overview

1.1 Background

The unwanted sound, noise, can lead to health problems, e.g. hearing loss and stress-related problems. A pre-knowledge of noise generation by machines is of great importance due to the ever-shorter product development cycles and stricter noise legislation. The noise from a machine radiates to the environment indirectly via the foundation structure and directly via the surrounding fluid, which is usually air. These indirect and direct noise radiations can also be coupled. A fluid machine converts the energy from the fluid into mechanical energy or vice versa. Examples of the fluid machines are internal combustion engines (IC-engines), pumps, compressors, and fans. A review of the modelling of fluid machines as sources of sound can be found in the paper by Bodén and Åbom [17]. They concluded that predicting and controlling noise from a fluid machine requires a model of the noise sources themselves, i.e. acoustic source data. If the source connects weakly to the surroundings, the standardized free field methods described in [49] can be used for the source sound power determination, i.e. source characterization. In terms of frequency, the weak coupling corresponds to high frequencies (wavelength/typical dimension $\gg$ 1), when power-based methods can be applied. For this high frequency range, the source sound power is constant, i.e. does not change with position. In the low or mid-frequency range (wavelength/typical dimension $\ll$ 1 or $\approx$1), strong coupling between a source and its surrounding can occur. This will lead to a variation of source sound power with position or change in boundary conditions. An important case where this can occur is duct systems connected to different fluid machines.

Above a certain frequency, i.e. first non-plane wave mode cut-on frequency, the sound pressure varies over the duct cross-section and non-plane waves are introduced. For a number of applications, the plane wave range dominates and the non-plane waves can be neglected. But, for machines connected to large ducts, e.g. cruise ships and power plants with exhaust pipe diameters of $\approx$1 m, the non-plane wave range is also important. For example, at a temperature of 450°C

the first non-plane wave cut-on frequency in a typical automotive exhaust pipe of $\varnothing$=50 mm is 6319 Hz, whereas in the medium speed IC-engine with an exhaust duct of $\varnothing$=1600 mm this frequency is only 197 Hz. Thus, the three-dimensional effect in the acoustic wave propagation cannot be neglected.

The gas dynamics of an IC-engine can essentially be described by a set of coupled non-linear equations for conservation of mass, momentum, and energy. The most widely used method to solve these non-linear equations in the time domain is to use a finite volume or finite difference method. The methods and examples concerning IC-engines are explained in-depth by Munjal [65] and by Winterbone and Pearson [79, 80], for example. The governing equations are often simplified by treating variables such as pressure, density, velocity, and temperature as constants over the duct cross-section, i.e. to use a one-dimensional (1D) model. 1D commercial process simulation software such as Boost [21], Wave [78], and GT-Power [34] are the most widely used within the automotive industry. These codes are mainly used to predict IC-engine performance quantities such as volumetric efficiency, torque, and power. In addition, the codes provide the pressure and flow velocities at the intake and exhaust system. The high frequency phenomena are so complicated, however, that it is practically impossible to simulate them accurately. Thus, in order to develop methods to estimate the sound produced, experimental studies are also essential. The challenge with the experiments is that the source characteristics are dependent on the acoustic load, and the sound power is reflected from the duct discontinuities as well as from the duct terminations. The sound pressure measurements might also be contaminated by the turbulence in the flow.

For the acoustic analysis of fluid machines, linear models are often preferred because of their computational efficiency and the accuracy of acoustic loss models. Using linear models, frequency domain analysis is a convenient way to design the sound transmission path elements, such as mufflers and silencers of the exhaust system as discussed by, e.g. Munjal [65]. To make a complete linear system model, acoustic load-independent source data (source strength & source impedance) is needed as an input in the frequency domain simulations.

There are also hybrid modelling approaches where the time domain and the frequency domain methods are combined. Several hybrid approaches have been reviewed in a state-of-the-art review of the acoustic source characterization of an IC-engine by Munjal [66] and in a paper by Albertson et al. [4]. The hybrid methods studied in these papers were found to be computationally expensive and rather complex.

Although the high level sound sources such as medium speed IC-engines indicate some non-linear behaviour, linear models have been found to give sufficiently good results, see e.g. [15, 18]. In this thesis, the duct acoustics are studied using linear frequency domain methods.

Acoustic multi-ports

As stated by Bodén and Åbom [17], in general, a linear time-invariant acoustic source can be described as an acoustic multi- or N-port. Here, linear refers to the structure of the governing equations describing the acoustic behaviour of a source. Time-invariant means that the operators or boundary conditions in the governing equations are independent of time. The properties of multi-ports are independent of the rest of the system, and the networks of the multi-ports describing sources and transmission elements can for the plane wave range be assembled using, for example, SIDLAB [26], which is a software developed for this purpose. In the case of duct systems with one input and one output and only plane waves which are acoustically coupled, the N-ports reduce to two-ports. Different formulations for the two-ports exist, described in the books by Pierce [71] and by Munjal [65], for example. Glav and Åbom [32] developed a general formalism for analysing the acoustics of networks consisting of acoustic two-ports.

The one-dimensional two-port data can be determined experimentally by measuring the scattering matrix as described by Åbom [2], for example. To perform two-port measurements, the acoustic velocity and pressure must first be determined or equivalently the travelling wave amplitudes. These properties can be measured using standardized methods; the standing wave ratio (SWR) or the two microphone method (TMM) [47, 48]. The SWR method can yield accurate results in a stationary medium, but it is very difficult to apply in practice; to characterize the exhaust noise of an IC-engine, for example. Using the TMM, a wall-mounted microphone configuration can be used. The results are poor when the distance between the two microphones is close to multiples of half a wavelength. Therefore, more than one microphone pair is used to cover a wider frequency range. A suitable way to determine the microphone separations have been suggested by Åbom and Bodén [3]. Also, the non-linear acoustic properties of the in-duct sample can be taken into account as recently shown by Bodén [13, 14]. In this thesis, using wall-mounted microphones, methods to determine the two-port data including also the non-plane waves are proposed.

Two-port models

Two-port simulation models for a number of elements used in the automotive exhaust systems can be found. Considering the after-treatment devices (ATD), which are studied in this thesis, Allam and Åbom presented models for diesel particulate filters (DPF) and automotive catalytic converters (CC) [5, 7, 8]. The models were also verified with measurements by Elnady et al. [29]. Elnady et al. also developed an approach to model the perforates in mufflers [27] and a technique also to take into account the flow and pressure drop in the calculations [28]. One of the first acoustic models of a CC was presented by Glav et al. [33]. The model was based on an ad hoc combination of a classic formula for damping in narrow pipes with no flow with a model for flow-induced damping. Dokumaci [24] made an improved model

by showing that the equations for sound propagation in a thermoviscous fluid simplified according to the Zwikker and Kosten theory [81] can be solved in the case of the circular pipe with plug flow. Later, Dokumaci extended the model for the rectangular cross sections [25]. Peat [68] and Astley and Cummings [10] used the finite element method (FEM) to study the sound attenuation and propagation in channels of arbitrary cross section with flow. Astley and Cummings concluded that the FEM results are consistent with classic no-flow solutions for circular tubes. The effect of the temperature gradients at the inlet of the CC has been studied by Peat [69] and by Peat and Kirby [70]. According to their results, the temperature gradients can have a marked effect on the sound attenuation. In a typical exhaust pipe of a medium speed IC-engine, the Mach number is approximately 0.06, see Paper I [46]. Taking into account also the fact that the area expansion at the after-treatment devices consisting of narrow pipes is quite large, it can be assumed that in practice the mean flow effects can be neglected. Based on the large area expansion, Allam and Åbom [16] proposed that, alternatively to the Dokumaci model, the two-port for the narrow pipe section can be calculated using the classic Kirchhoff solution presented by Keefe [56] for the circular pipes and by Stinson [77] for narrow pipes of arbitrary cross-section. As stated by Allam and Åbom [16], using the hydraulic diameter in the classic Kirchhoff solution gives similar results to the Stinson formulation within 2% when the aspect ratio of the capillary is reasonable. All of these simulation models are based on one-dimensional plane wave assumption. By using a power flow formulation, see section 2.3, one can formally extend the two-port model for ducted elements beyond the plane wave range. This approach has been applied in this thesis to analyse after-treatment devices, see section 2.4.

Acoustic one-port source

If there is only one degree of freedom between the source and the rest of the system, the one-port model can be used. To characterize an IC-engine as an acoustic one-port source, it is possible to use multi-load methods [12], for example. Measuring the source data using the multi-load method would require several different acoustic loads, which means major changes to the exhaust system and is, therefore, both costly and time consuming. It has been demonstrated that using the nonlinear, time domain, commercial codes, the linear, frequency domain, plane wave frequency range, in-duct source characteristics in automotive engine intakes [58] and exhausts [38] can be determined. In this thesis, this approach is applied for the first time to a medium speed IC-engine. In addition, power-based methods to determine high frequency one-port source data are also investigated.

Medium speed IC-engine exhaust system

The purpose of the exhaust gas line of a medium speed IC-engine is to reduce the pollutants from the exhaust gases and reduce the noise emissions. Also the energy from the gas can be recovered. The back pressure of the whole exhaust gas

line must remain reasonable so as not to decrease the engine efficiency [76]. The thermal energy from the exhaust gas is recovered with boilers. The silencers are usually designed to reduce the noise emissions at certain frequencies, e.g. engine harmonics. With the scrubber, unwanted pollutants such as sulphur oxides (SO_x) are washed away with liquids. The nitrogen oxide (NO_x) reduction takes place in the selective catalytic reducer (SCR). In the oxidation catalyst (OC), the carbon monoxide (CO) and hydrocarbon (HC) components are removed. As input data for designing silencer systems for large exhaust pipes and medium speed engines, the sound power from the engine under reflection-free conditions is a common alternative suggested in standards and handbooks. Assuming that this sound power is known, the sound attenuation of the complete exhaust gas line can be estimated with software packages designed for that purposes, e.g. the compact silencer system (CSS) [11, 35].

Due to large unmovable constructions and a harsh environment, it is practically impossible to measure the exhaust noise of a medium speed IC-engine in a reflection-free environment as proposed in the standardized methods to determine the radiated sound power by fans and other air-moving devices [51]. Alternatively, if the acoustic load is known, the source data could be estimated by measuring the transmitted sound power exterior to the duct, i.e. from the exhaust duct outlet. Unfortunately, due to the unknown properties of the system under operating conditions these measurements are uncertain. There are also uncertainties in the directivity of the exhaust noise radiation from the tailpipe(s). In addition, the external measurements are dependent on the weather conditions.

The second alternative is the in-duct measurements, which are examined in this thesis. Conventionally, the source data for CSS [35] simulations are approximated by measuring the in-duct sound pressures using one microphone, discarding the reflections [53]. In this thesis, the low frequency plane wave source characteristics for a medium speed IC-engine exhaust system are obtained by simulating the acoustic multi-load method measurements and are validated with engine performance and cylinder pressure measurements. The one-port high frequency in-duct source characteristics of the test IC-engine are determined *in situ* with wall-mounted microphones.

It is known from earlier studies [7, 29] that the transmission loss of a typical ATD unit can be quite significant. An ATD unit for diesel engines is classically assembled from several specific parts such as SCR, OC and diesel particulate filters (DPF). One new alternative to the conventional DPF is the particle oxidation catalyst (POC®). The substrate used in the X type POC® (POC-X) filter consists of fine, corrugated metallic wire mesh screens piled askew and rolled into a cylindrical shape. In order to analyse the ATD with SCR or OC acting as a reactive or dissipative noise attenuation element in the exhaust gas line, the coupled system of the wave propagation in the channels and in the cavity must be solved. Selamet et al. [75] used analytical and FEM approaches so as to determine the wave attenuation of automotive CC taking into account the coupled system. They concluded that, for the frequency range of interest in automotive applications, the wave propagation is

predominantly one-dimensional and the three-dimensional effect can be neglected. Christoffersen et al. [22] combined the SCR and silencer of a large diesel engine exhaust system. They used a 1D in-house code for the acoustic modelling of the combined system. As a conclusion, they emphasized that the mixing pre chamber of the SCR can contribute significantly to the system attenuation.

Using the methods proposed in the thesis, the low and mid-frequency range noise attenuation of a medium speed IC-engine ATD is obtained taking into account the non-plane waves. For the POC-X, acoustic two-port simulation models are proposed.

Measurements

Above the first non-plane wave mode cut-on frequency, the sound pressure varies over the duct cross-section, and non-plane waves are introduced. Traditionally, this cut-on frequency is determined using the speed of sound, which is estimated from temperature. In industrial applications, the temperature, humidity and composition of the fluid varies and, therefore, the speed of sound is not constant. With the full plane wave decomposition (FWDM) suggested by Allam and Åbom [6], the complex wave amplitudes and wave numbers taking into account damping can be determined using an array of at least four microphones. If the damping is neglected, the complex wave amplitudes and the speed of sound can be determined by measuring the acoustic pressures from three axial positions of the duct as suggested by Lavrentjev and Tiikoja [59]. In this thesis, an alternative to the previous works [6, 59], using the cut-on frequency for the first mode to determine the sound speed, is proposed.

When considering the non-plane wave range, the acoustic excitation is a superposition of several in-duct modes. In addition the reflection of the sound, e.g. at an opening as studied by Jurkiewicz et al. [55], will create modal coupling. For this reason, measuring the high frequency modal reflections accurately becomes complicated. However, for the application studied in this thesis measurements are often taken upstream of large dissipative silencers. Under these circumstances, the termination can for high frequencies be seen as “reflection-free”. The high frequency source data can then be estimated with the measured in-duct sound power.

Of course, the relationship between measured sound pressure and the in-duct sound power is not simple. Bolleter and Crocker [20] and Bolleter et al. [19] studied several microphone arrangements and modal participation factors when estimating the modal spectra and sound generation by ducted fans or compressors. They concluded that the modal power spectra can be predicted with reasonable accuracy if the radial position of the microphones can be set arbitrarily. They also concluded that the flow noise can be suppressed using a long cylindrical windscreen, i.e. a Friedrich tube, when measuring the pressure fluctuations in the duct. Due to the high temperature in the exhaust duct of an IC-engine, using the slit tube method or measuring the pressure from various radial locations in the duct is not possible.

According to Joseph et al. [54], determination of sound power from the pressure measurements is possible when there is *a priori* knowledge of the source distribution. Unfortunately, the source distribution is rarely known and the distribution must be idealized. Joseph et al. [54] also investigated the relationship between pressure and power for a number of idealized source distributions in an infinite duct. Their calculations show that a well-defined high frequency asymptote exists only for the source distribution of equal energy per mode and for axial dipole distribution in the absence of flow. The sound power determination in hard-walled pipes was studied by Michalke [62, 63]. Based on the theoretical results of the propagation of sound generated by various types of sources shown in [62], the aim in [63] was to study how the sound power spectrum, by means of pressure measurements, can be determined without assumptions about the nature of the sound field to be measured. As an alternative to the standard method [51], Michalke proposed sound power determination via the area-averaged cross-spectral density of sound pressure using microphones at N_r different radial positions. Michalke concluded that the system cannot be solved satisfactorily at higher frequencies (Helmholtz number $He = kR > 8$, where k is the wave number and R is the radius of the duct) and the total number of measurements increases rapidly with the frequency. Later, Arnold [9] measured the area-averaged cross-spectra for a number N_ϕ equidistant angular microphone positions. In this way, he extended the useful frequency range up to Helmholtz number $kR = 30$. The standardized in-duct method to determine the sound power radiated into a duct by fans and other air-moving devices [51] is based on the above-mentioned papers. Neise and Arnold [67] revised the standard and proposed new modal correction data to obtain the higher frequency sound power. In this thesis, the sound pressures are measured using wall-mounted microphones and therefore the above-mentioned method cannot be used. Instead, a new procedure is proposed based on both experimental tests and numerical simulations.

Finally, to get the sound power for reflection-free conditions at all frequencies, the source characteristics in the low frequency plane wave range are combined with those in the high frequency non-plane wave range. As stated by Gijrath and Åbom [31], the power-based approach is only relevant in a frequency averaged sense and for frequencies where the number of propagating modes is large. In this thesis, the non-plane wave frequency range in-duct sound power is estimated using 1/3 octave frequency band sound power weighting factors for multi-modal excitations.

The aim is to find the best three-microphone configuration which can be used with wall-mounted microphones not only in the plane wave range but also to estimate the high frequency non-plane wave range acoustic power. This approach can then be used not only for source characterization but also for determining damping with non-plane waves for transmission path elements such as catalyzers, for example.

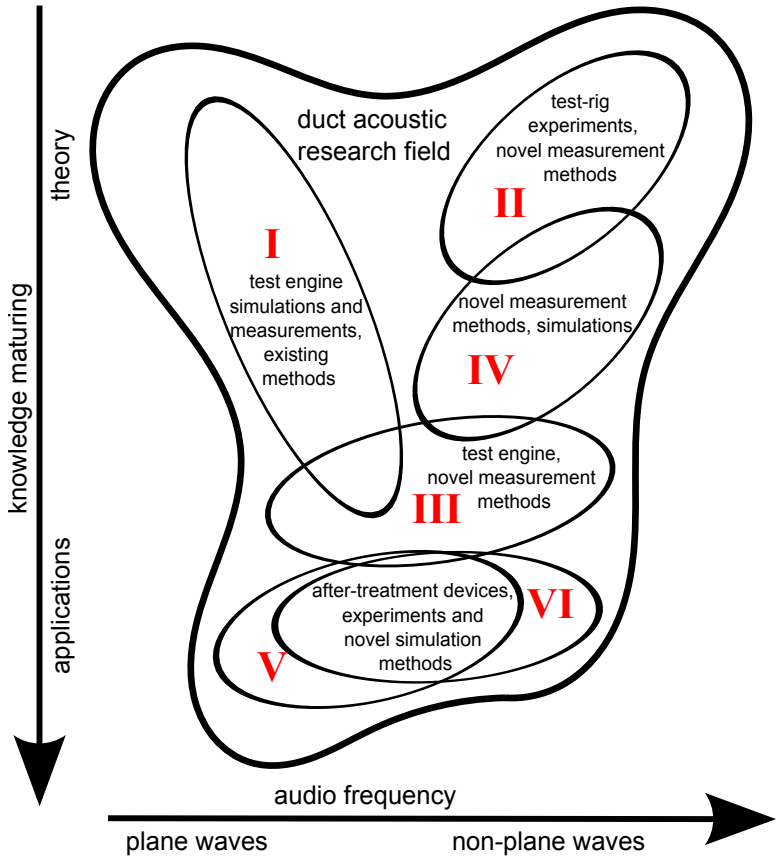

Figure 1.1: Illustration of the relations between the papers in the thesis and theory/applications as well as frequency domain on the duct acoustic research field. The ovals in the figure describe the papers included in this thesis.

1.2 Organisation of the thesis

The relations between the six papers on which this thesis is built are illustrated in Fig. 1.1. In the figure, the horizontal axis describes the audio frequency range, which in duct acoustics can be divided into the low frequency range with plane waves and into the high frequency range with non-plane waves. The vertical axis describes the knowledge maturing. In the beginning (top), there are various theories from which the most relevant ones are investigated further. Using simulations and experimental methods, the knowledge is finally matured to be useable with real applications (bottom).

In Paper I [46], the plane wave range acoustic source characterization methods are applied to a medium speed IC-engine exhaust system using simulations and the results are validated with measurements. In Paper II [39], the novel measurement methods and the dependency of the high frequency in-duct source characteristics from the excitation source type is investigated experimentally. The novel high frequency range measurement methods are studied theoretically and with simulations in Paper IV [43]. The theory for the low and high frequency source data combination is shown and applied to the test engine in Paper III [41]. Methods to determine the two port data with non-plane waves for the after-treatment devices are proposed in papers V and VI [40, 42].

Chapter 2

Theory

2.1 Duct acoustics

The acoustic wave propagation in a medium can be described by the time harmonic convected inhomogeneous wave equation

$$\left(\frac{1}{c_0^2}\frac{D_0^2}{Dt^2} - \nabla^2\right)p = \frac{D_0 m}{Dt} - \nabla\cdot(\mathbf{f} - m\mathbf{U}), \tag{2.1}$$

where p is the acoustic pressure, c_0 is the speed of sound, $\frac{D_0}{Dt} = \frac{\partial}{\partial t} + \mathbf{U}\cdot\nabla$ is the convective derivative, $\mathbf{U}$ is the mean flow velocity. The right hand side of Eqn. (2.1) describes the source terms. The first contribution of the right hand side can be seen as a monopole source and the remaining as dipole sources. m is mass and $\mathbf{f}$ describes external forces. By solving Eqn. (2.1) with different sources, the frequency response can be determined.

In a duct, only a finite set of shapes "modes" for transversal pressure field can propagate. The solution to the wave equation in a uniform circular straight duct can be written as a superposition of modal pressures as

$$\hat{p}(x,\mathbf{r}) = \sum_{(m,n)} \hat{p}_{mn}(x,\mathbf{r}), \tag{2.2}$$

where x is the coordinate along the duct axis, $\mathbf{r}$ is the position vector over the duct cross-section and m, n are the number of radial and circumferential nodal lines of the modal pressure field $\hat{p}_{mn}$, respectively. According to Munjal [65] for example, the modal pressures can be described using the downstream and upstream propagating waves as

$$\hat{p}_{mn}(x,\mathbf{r}) = \hat{p}_{mn+}\psi_{mn+}(\mathbf{r})e^{-jk_{xmn+}x} + \hat{p}_{mn-}\psi_{mn-}(\mathbf{r})e^{jk_{xmn-}x}, \tag{2.3}$$

where $\hat{p}_+$ and $\hat{p}_-$ are the complex valued acoustic pressures propagating downstream (+) and upstream (−), ψ_+ and ψ_- are the eigenfunctions which depend on

Table 2.1: Nodal lines for in-duct acoustic pressure distribution of some non-plane wave acoustic modes in a circular duct and corresponding Helmholtz cut-on frequencies.

He	1.84	3.05	3.83	4.20	5.32	5.33
(m,n)	1,0	2,0	0,1	3,0	4,0	1,1
	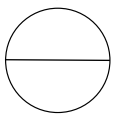	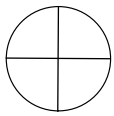	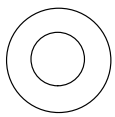	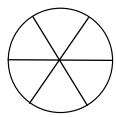	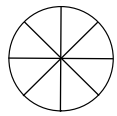	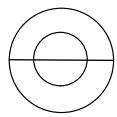

the cross-section shape and k_+ and k_- are the wave numbers. For uniform flow and rigid walls, the wave numbers are defined as

$$k_{xmn\pm} = \frac{\mp M k_0 + \sqrt{k_0^2 - (1-M^2)k_{rmn}^2}}{1-M^2}, \tag{2.4}$$

where M is the Mach number, k_0 is the ordinary wave number, and k_{rmn} are the well-known transversal wave numbers. For the case of uniform flow, the modes can also be assumed to be orthogonal and equal, i.e., $\psi_{mn+} = \psi_{mn-}$. The nodal lines of some non-plane wave modes and corresponding Helmholtz cut-on frequencies $He = k_{rmn}R$, where R is the radius of the duct, are shown in Table 2.1. Below cut-on, the modes are exponentially damped in their direction of propagation, i.e. they represent nearfields and carry no acoustic power. Above cut-on, they propagate as waves and transport acoustic power.

The corresponding speeds of the downstream and upstream propagating wave modes are

$$c_{mn\pm} = \frac{\omega}{k_{xmn\pm}}. \tag{2.5}$$

The acoustic velocity field can be written as a superposition of modal acoustic velocities

$$\hat{u}(x,\mathbf{r}) = \sum_{(m,n)} \hat{u}_{mn}(x,\mathbf{r}). \tag{2.6}$$

assuming a small Mach number case the modal pressures and velocities are related via:

$$\hat{u}_{mn}(x,\mathbf{r}) = \frac{\hat{p}_{mn+}}{\rho c_{mn+}}\psi_{mn+}(\mathbf{r})e^{-jk_{xmn+}x} - \frac{\hat{p}_{mn-}}{\rho c_{mn-}}\psi_{mn-}(\mathbf{r})e^{jk_{xmn-}x}. \tag{2.7}$$

2.2 Plane wave two-ports

If we assume a linear sound field theory to be valid, the transfer matrix formulation can be used to describe the frequency domain relationship between the acoustic

states at the inlet and outlet of the two-port as

$$\left\{ \begin{array}{c} \hat{p}_{in} \\ \hat{q}_{in} \end{array} \right\} = \left[\begin{array}{cc} T_{11} & T_{12} \\ T_{21} & T_{22} \end{array} \right] \left\{ \begin{array}{c} \hat{p}_{out} \\ \hat{q}_{out} \end{array} \right\}, \tag{2.8}$$

where $\hat{p}$ and $\hat{q}$ are the fourier transforms of the plane wave acoustic pressure and volume velocity at the inlet and outlet as denoted with subscripts *in* and *out*, respectively. The elements T_{xy} of the transfer matrix $\mathbf{T}$ describe the sound reflections and transmissions of the passive system. Using this formulation, the internal sound sources are neglected. Using the transfer matrix formalism, M passive elements in a cascade can be assembled easily by multiplying the corresponding transfer matrices $\mathbf{T}_m$

$$\mathbf{T}_{tot} = \prod_{m=1}^{M} \mathbf{T}_m. \tag{2.9}$$

Using travelling waves as the state variables instead of the acoustic pressure and the volume velocity as presented by Glav and Åbom [32] leads to the scattering matrix formalism. If we define the waves to be positive when travelling out of the port, the two-port elements of the multi-port network can be written as

$$\left\{ \begin{array}{c} \hat{p}_{1+} \\ \hat{p}_{2+} \end{array} \right\} = \left[\begin{array}{cc} S_{11} & S_{12} \\ S_{21} & S_{22} \end{array} \right] \left\{ \begin{array}{c} \hat{p}_{1-} \\ \hat{p}_{2-} \end{array} \right\} + \left\{ \begin{array}{c} \hat{p}_{1s+} \\ \hat{p}_{2s+} \end{array} \right\}, \tag{2.10}$$

where S_{xy} are the elements of the scattering matrix $\mathbf{S}$, subscript s describes the source and subscripts $+$ and $-$ indicates the direction of the wave propagation. The scattering matrix formalism is more general than the classic transfer matrix formalism, because it can be applied to the systems with sources anywhere in the network. Using some algebra, the transfer matrix $\mathbf{T}$ converts into the scattering matrix $\mathbf{S}$ via

$$\mathbf{S} = \left[\begin{array}{cc} T_{21}/T_{11} & T_{22} - T_{12}T_{21}/T_{11} \\ 1/T_{11} & -T_{12}/T_{11} \end{array} \right]. \tag{2.11}$$

Correspondingly, the scattering matrix $\mathbf{S}$ converts into the transfer matrix $\mathbf{T}$ via

$$\mathbf{T} = \left[\begin{array}{cc} 1/S_{21} & -S_{22}/S_{21} \\ S_{11}/S_{21} & S_{12} - S_{11}S_{22}/S_{21} \end{array} \right]. \tag{2.12}$$

Only the plane waves are allowed to propagate at the inlet and outlet of the two-ports described with the transfer matrix $\mathbf{T}$ or with the scattering matrix $\mathbf{S}$. However, the acoustic field inside the system can be more complicated, including three-dimensional phenomena.

Low frequency source characteristics

The sound from an acoustic one-port source propagates in the duct in the downstream and upstream direction as illustrated in Fig. 2.1. In the frequency domain,

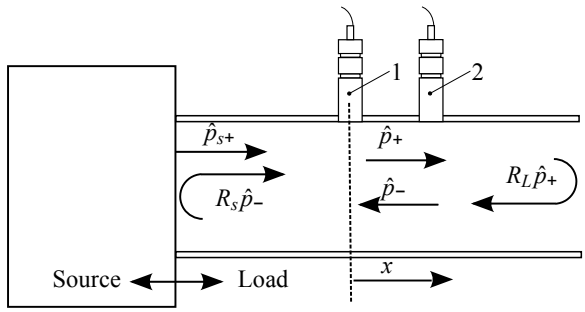

Figure 2.1: Schematic of the acoustic one-port source and the propagating waves. In the low frequency plane wave range, the downstream (+) and upstream (−) propagating waves can be separated using the two-microphone method.

the measured sound pressure at the cross section x is

$$\hat{p}_{0x} = \hat{p}_{0+}e^{-ik_+x} + \hat{p}_{0-}e^{ik_-x}, \tag{2.13}$$

where $\hat{p}_+$ and $\hat{p}_-$ are the complex acoustic pressures propagating downstream (+) and upstream (−), subscript 0 denotes the plane wave modes, and k is the wave number. In the low frequency plane wave range, these waves can be separated with the widely used two-microphone method, i.e., via determination of the load reflection coefficient at the cross section $x = 0$

$$R_L = \frac{\hat{p}_{0-}}{\hat{p}_{0+}} = \frac{H_{12} - e^{-ik_+s}}{e^{ik_-s} - H_{12}} \tag{2.14}$$

by measuring the transfer functions H_{12} between the two microphones, separated by distance s from each other. The two-microphone method is detailed by e.g. Chung and Blaser [23] and also used in the standardized methods to determine, for example, the sound absorption coefficient [48]. A suitable way to determine the microphone separations in order to minimize the error sensitivity has been suggested by Åbom and Bodén [3].

Part of the upstream propagating sound is also reflected from the source, $R_s\hat{p}_-$ in Fig. 2.1. As stated by Bodén and Åbom [17], the acoustic one-port source can be described fully by source strength $\hat{p}_{s+}$ together with the source reflection coefficient R_s. The downstream propagating wave is, therefore, the sum of the outgoing source strength and the wave reflected from the source

$$\hat{p}_{0+} = \hat{p}_{s+} + R_s\hat{p}_{0-}, \tag{2.15}$$

and using Eqn. (2.14) in Eqn. (2.15), the outgoing source strength at the source cross section becomes

$$\hat{p}_{s+} = \hat{p}_{0+}(1 - R_sR_L), \tag{2.16}$$

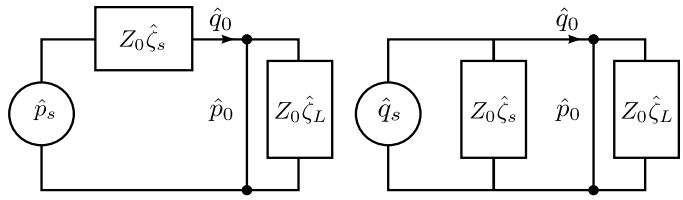

Figure 2.2: Electro-acoustic analogy for a linear time-invariant one port source model. Pressure source (left), volume velocity source (right).

where the downstream acoustic pressure can be solved from Eqns. (2.13) and (2.14), that is

$$\hat{p}_{0+} = \frac{\hat{p}_{0x} e^{ik_+ x}}{1 + R_L e^{ix(k_+ + k_-)}}. \tag{2.17}$$

Direct determination of the source data

In some cases, the acoustic source data can be measured directly. First, the acoustic source studied is excited with an external source and the source reflections R_s are measured. Then, the external source is turned off and the pressure response for a known termination R_L is determined. The outgoing source strength $\hat{p}_{s+}$ can then be determined from Eqn. (2.16). In the case of fairly low noise machines, e.g. fans or compressors, this direct method is useable.

The problem when focusing on the IC-engines is that the external acoustic source must be more powerful than the primary source. Unfortunately, as stated by Gupta and Munjal [36], IC-engines produce such high sound pressure levels in the low frequency range that it is practically impossible to construct external sources that overcome the primary source.

Indirect determination of the source data

When applying the indirect methods, the electro-acoustic analogy shown in Fig. 2.2 is usually used to formulate the equations.

The acoustic pressure and volume velocity are related to each other via the analogy [65] as

$$\hat{p}_s = \hat{p}_0 + Z_0\hat{\zeta}_s\hat{q}_0, \tag{2.18}$$

and

$$\hat{q}_s = \frac{\hat{p}_0}{Z_0\hat{\zeta}_s} + \frac{\hat{p}_0}{Z_0\hat{\zeta}_L} \tag{2.19}$$

in the case of pressure source $\hat{p}_s$ and volume velocity source $\hat{q}_s$ respectively. In Eqns. (2.18) and (2.19), $Z_0 = \rho c/S$ is the characteristic impedance for a propagating plane wave in a duct with cross-sectional area S filled with gas of density ρ, c is

the speed of sound, and $\hat{\zeta}_s$ and $\hat{\zeta}_L$ are the normalized source and load impedances respectively.

For a linear and time-invariant system, the pressure and volume velocity are related via

$$\hat{p}_s = \hat{q}_s Z_0 \hat{\zeta}_s \tag{2.20}$$

and

$$\hat{p}_0 = \hat{q}_0 Z_0 \hat{\zeta}_L \tag{2.21}$$

in the case of source impedance and acoustic load impedance respectively. Finally, using Eqns. (2.18) and (2.21), the acoustic pressure can be written as

$$\hat{p}_0 = \frac{\hat{p}_s \hat{\zeta}_L}{\hat{\zeta}_s + \hat{\zeta}_L}. \tag{2.22}$$

By applying N known acoustic load impedances $\hat{\zeta}_{Ln}$ to the system and measuring the corresponding acoustic pressures $\hat{p}_{0Ln}$, the source data can be solved. This is called the multi-load method [12]. Since there are only two unknowns, two loads should be sufficient, i.e., $n = 1...2$. This leads to the two-load method. In the case of a pressure source model, the resulting system of equations in matrix form becomes

$$\begin{bmatrix} \hat{\zeta}_{L1} & -\hat{p}_{0L1} \\ \hat{\zeta}_{L2} & -\hat{p}_{0L2} \end{bmatrix} \begin{Bmatrix} \hat{p}_s \\ \hat{\zeta}_s \end{Bmatrix} = \begin{Bmatrix} \hat{p}_{0L1}\hat{\zeta}_{L1} \\ \hat{p}_{0L2}\hat{\zeta}_{L2} \end{Bmatrix}. \tag{2.23}$$

Nowadays, the multi-load method is also implemented in commercial IC-engine simulation codes widely used within the automotive industry. In Paper I [46], the low frequency plane wave acoustic source data of a medium speed IC-engine exhaust system is determined using GT-Power software and ten different acoustic loads. The simulated source data is validated comparing with experimental data for the same engine.

Taking into account the reflection-impedance relations on the source side

$$\hat{\zeta}_s = \frac{1 + R_s}{1 - R_s}, \tag{2.24}$$

and on the load side

$$\hat{\zeta}_L = \frac{1 + R_L}{1 - R_L}, \tag{2.25}$$

and plugging these into Eqn. (2.22) and using Eqn. (2.16), the relation between the electro-acoustic analogy source strength $\hat{p}_s$ and the outgoing source strength $\hat{p}_{s+}$ is

$$\hat{p}_s = \hat{p}_{s+} \frac{2}{1 - R_s}. \tag{2.26}$$

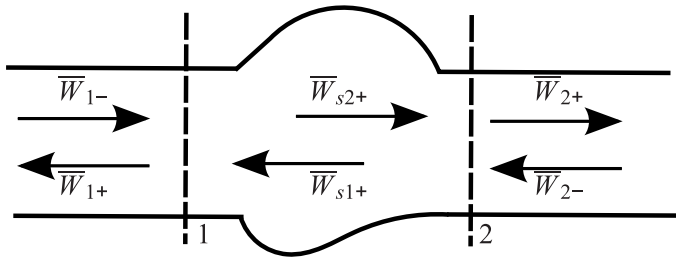

Figure 2.3: Directions of the sound power flow in an acoustic two-port. The power is positive when flowing out of the port.

2.3 Frequency range extension using sound power formulation

If we use travelling sound powers as the state variables as proposed by Gijrath and Åbom [31], the scattering matrix formalism can be extended into the higher frequency non-plane wave range. Defining the sound power to be positive when flowing out of the port, as shown in Fig. 2.3, the power-scattering matrix equation becomes

$$\left\{ \begin{array}{c} \overline{W}_{1+} \\ \overline{W}_{2+} \end{array} \right\} = \left[\begin{array}{cc} S_{p11} & S_{p12} \\ S_{p21} & S_{p22} \end{array} \right] \left\{ \begin{array}{c} \overline{W}_{1-} \\ \overline{W}_{2-} \end{array} \right\} + \left\{ \begin{array}{c} \overline{W}_{s1+} \\ \overline{W}_{s2+} \end{array} \right\}, \tag{2.27}$$

where $\overline{W}$ is the time-averaged sound power, the elements S_{pxy} of the power-scattering matrix $\mathbf{S_p}$ describe the sound power reflections and the sound power transmissions of the two-port. Note that also the power-scattering matrix $\mathbf{S_p}$ can be converted into the power transfer matrix form $\mathbf{T_p}$ and vice versa. The advantage of the power-scattering matrix formalism is that it is not limited to the plane wave frequency range.

Acoustic sound power one-port

In order to describe the IC-engine as an acoustic source, the second port can be discarded and the two-port Eqn. (2.27) reduces into a one-port

$$\overline{W}_{+} = \overline{W}_{s+} + R_{ps}\overline{W}_{-}, \tag{2.28}$$

where the subscript describing the port number is omitted for clarity.

If the sound power reflection and transmission coefficients for all elements as well as the source characteristics are defined, the whole system can be assembled and solved. The medium speed IC-engine source characteristics including the high frequency range are studied in Paper III [41]. It was concluded that the source

terms in Eqn.(2.27) can be calculated piecewise by

$$\overline{W}_{s+} = \begin{cases} \overline{W}_{s+}^{LF} & , f < f_{10,cut-on} \\ \\ \overline{W}_{s+}^{HF} & , f \geq f_{10,cut-on}, \end{cases} \tag{2.29}$$

where the superscripts LF and HF describe the low and high frequency ranges respectively, and f_{10} denotes the first non-plane wave mode cut-on frequency inside the duct, i.e. the mode with one radial and zero circumferential nodal lines starts to propagate at that frequency. That is

$$f_{10,cut-on} = \frac{k_{r10}c}{2\pi}\sqrt{1-M^2}, \tag{2.30}$$

where the transversal wave number k_{r10} comes from the first zero of the derivative of the Bessel function ($J_1' = 0$). Above this limit, the source power can be estimated with the help of 1/3 octave frequency band weighting factors studied in Papers II and IV [39, 43].

The time-averaged in-duct acoustic power is defined as

$$\overline{W} = \int \overline{I} dS, \tag{2.31}$$

where $\overline{I}$ is the time-averaged intensity in the axial direction and S is the cross-sectional area of the duct. For the harmonic and complex valued signals the time-averaged active intensity is given by [64]

$$\overline{I} = (1+M^2)\frac{1}{2}Re(\hat{p}\hat{u}^*) + M\left(\frac{|\hat{p}|^2}{2\rho c} + \frac{\rho c|\hat{u}|^2}{2}\right), \tag{2.32}$$

where $\hat{u}$ is the acoustic velocity and $*$ denotes the complex conjugate. Opening the term $\hat{p}\hat{u}^*$ in Eqn. (2.32) modalwise leads to

$$\begin{aligned} \hat{p}_{mn}\hat{u}_{mn}^* = &\frac{\hat{p}_{mn+}\psi_{mn+}(\mathbf{r})e^{-jk_{xmn+}x}(\hat{p}_{mn+}\psi_{mn+}(\mathbf{r})e^{-jk_{xmn+}x})^*}{(\rho c_{mn+})^*} - \\ &\frac{\hat{p}_{mn+}\psi_{mn+}(\mathbf{r})e^{-jk_{xmn+}x}(\hat{p}_{mn-}\psi_{mn-}(\mathbf{r})e^{jk_{xmn-}x})^*}{(\rho c_{mn-})^*} + \\ &\frac{\hat{p}_{mn-}\psi_{mn-}(\mathbf{r})e^{jk_{xmn-}x}(\hat{p}_{mn+}\psi_{mn+}(\mathbf{r})e^{-jk_{xmn+}x})^*}{(\rho c_{mn+})^*} - \\ &\frac{\hat{p}_{mn-}\psi_{mn-}(\mathbf{r})e^{jk_{xmn-}x}(\hat{p}_{mn-}\psi_{mn-}(\mathbf{r})e^{jk_{xmn-}x})^*}{(\rho c_{mn-})^*}. \end{aligned} \tag{2.33}$$

After some algebra, we can write

$$\begin{aligned} \frac{1}{2}Re(\hat{p}\hat{u}^*) = \sum_{(m,n)} \Bigg[&\frac{|\hat{p}_{mn+}\psi_{mn+}(\mathbf{r})|^2}{2} Re\left(\frac{1}{(\rho c_{mn+})^*}\right) - \\ &\frac{|\hat{p}_{mn-}\psi_{mn-}(\mathbf{r})|^2}{2} Re\left(\frac{1}{(\rho c_{mn-})^*}\right)\Bigg]. \end{aligned} \tag{2.34}$$

Note that the terms $|\hat{p}|^2$ and $|\hat{u}|^2$ in Eqn. (2.32) can also be written modalwise using Eqns. (2.3) and (2.7).

Neglecting the flow, which is according to Paper I [46], reasonable assumption for medium speed IC-engine exhaust systems, the acoustic in-duct power is written as a function of travelling waves using Eqn. (2.34) as

$$\overline{W} = \int \sum_{(m,n)} Re\left(\frac{1}{\rho c_{mn}}\right) |\psi_{mn}(\mathbf{r})|^2 \left(\tilde{p}^2_{mn+} - \tilde{p}^2_{mn-}\right) dS, \tag{2.35}$$

where $\tilde{p}$ is the root mean square (RMS) of the acoustic pressure. Below the first non-plane wave cut-on frequency the sound pressure is constant over the duct cross-section and varies only longitudinally, that is the plane wave mode shapes equals unity. The plane waves in the exhaust system propagate with the speed of sound, i.e., $c_{mn} = c$ in Eqn. (2.35). For real valued density and speed of sound, i.e. for an ideal lossless fluid, the acoustic power in the plane wave frequency range simplifies into

$$\overline{W}^{LF} = \frac{S}{\rho c}(\tilde{p}^2_+ - \tilde{p}^2_-). \tag{2.36}$$

Using this formulation and considering only the downstream source pressure, the low frequency (LF) plane wave range outgoing (reflection-free termination) source power becomes

$$\overline{W}^{LF}_{s+} = \frac{|\hat{p}_{s+}|^2 S}{2\rho c}. \tag{2.37}$$

At the higher frequency range with non-plane waves, the acoustic wave propagation consists of several in-duct modes. If we define the modal power weighting factors as

$$\varepsilon_{mn} = \frac{\rho c}{S} \int Re\left(\frac{1}{\rho c_{mn}}\right) |\psi_{mn}(\mathbf{r})|^2 dS, \tag{2.38}$$

the non-plane wave acoustic power can be estimated as

$$\overline{W}^{HF} = \frac{S}{\rho c} \sum_{(m,n)} \varepsilon_{mn} (\tilde{p}^2_{mn+} - \tilde{p}^2_{mn-}). \tag{2.39}$$

The multi-modal wave propagation in a duct is rather complicated and according to, e.g. Jurkiewicz et al. [55] the reflected waves consist of their transformations in all possible modes of the same circumferential order. Typically, a resistive silencer is used in the IC-engine exhaust system, and we can assume the combined reflections from the silencer and the open termination to be negligible for high frequencies. Therefore, we do not need to solve the multi-modal reflections and transformations, and we can concentrate on the downstream propagating (+) part of Eqn. (2.39) (in addition to the plane waves).

Acoustic power weighting factors

The mode density increases with the frequency and detection of the propagating higher acoustic modes and the modal power weighting factors ε_{mn} becomes cumbersome. One alternative is to estimate the high frequency in-duct acoustic power in a frequency averaged sense. In Paper II [39], the high frequency non-plane wave acoustic power was determined experimentally and the high frequency in-duct acoustic power using 1/3 octave frequency band acoustic power weighting factors were estimated. In the experiments, monopole, dipole and quadrupole excitations were used. However, the source of a typical duct acoustic problem is seldom known exactly. When studying the exhaust noise of an IC-engine for example, the number of vanes and blades of a turbocharger affects the excitation, the source pressure distribution might also rotate and some modes could be excited particularly strongly. Using a non-symmetric volume acceleration (monopole) type of source, the excitation can be considered multi-modal, i.e. exciting all possible in-duct modes. Using this multi-modal frequency averaged approach, the sum of the modes in 1/3 octave frequency bands can be estimated by weighting the corresponding 1/3 octave frequency band total in-duct acoustic pressure with corresponding acoustic power weighting factors, that is

$$\left\langle \sum_{(m,n)} \varepsilon_{mn} \tilde{p}^2_{mn+} \right\rangle_{1/3} = \varepsilon_{1/3} \langle \tilde{p}^2_{tot} \rangle_{1/3}, \tag{2.40}$$

where $\langle\ \rangle_{1/3}$ denotes the summing over 1/3 octave bands, $\varepsilon_{1/3}$ is the acoustic power weighting factor, and $\tilde{p}_{tot}$ is the total RMS acoustic pressure. Plugging this into Eqn. (2.39) leads to

$$\overline{W}^{HF} = \frac{S}{\rho c} \varepsilon_{1/3} \langle \tilde{p}^2_{tot} \rangle_{1/3}. \tag{2.41}$$

If we know the total acoustic in-duct pressure and sound power, the power weighting factors can be derived. This challenge is discussed in the following sections.

In-duct sound power measurements

The flow in the exhaust duct is highly turbulent, which induces incoherent noise in the high frequency range. This noise is not suppressed when measuring the auto-spectra using wall-mounted microphones, which is the conventional way to measure the in-duct exhaust noise [11]. As stated by Rubiola and Vernotte [72], if a noisy system is measured simultaneously with two instruments, it is possible to extract the system spectrum from the background noise by averaging the cross-spectra.

The expectation of the square of the total acoustic pressure from the wall-mounted microphones can, therefore, be derived from the average cross-spectra

$$\mathbb{E}\{\tilde{p}^2_{tot}\} = \frac{1}{N} \sum_{x=1}^{n-1} \sum_{y=x+1}^{n} |S_{xy}|, \tag{2.42}$$

where N depends on the number of microphones used n, i.e. $N = n(n-1)/2$ and S_{xy} is the cross-spectrum between the microphones x and y. Using Eqns. (2.41) and (2.42), the high frequency in-duct acoustic power estimate is written as

$$\overline{W}^{HF} = \frac{S}{\rho c}\varepsilon_{xy,1/3}\left\langle \frac{1}{N}\sum_{x=1}^{n-1}\sum_{y=x+1}^{n}|S_{xy}| \right\rangle_{1/3}, \tag{2.43}$$

where $\varepsilon_{xy,1/3}$ is the 1/3 octave band acoustic power weighting factor for the cross-spectra of wall-mounted microphones. This way, the plane wave formula Eqn. (2.36) is extended into a higher, non-plane wave frequency range in 1/3 octave bands. These sound power weighting factors with error estimates are derived using simulations in Paper IV [43].

Sound power-scattering matrix

The challenge is to define the sound power reflection and transmission coefficients, i.e. matrix $\mathbf{S_p}$ of the subelements, e.g., ATD used in the medium speed IC-engine exhaust systems. With non-reflecting boundary condition at the outlet, $\overline{W}_{2-} = 0$, the sound power reflection and transmission coefficients can be derived from Eqn. (2.27) as

$$S_{p11} = \left(\frac{\overline{W}_{1+}}{\overline{W}_{1-}}\right)_{\overline{W}_{2-}=0}, \tag{2.44}$$

and

$$S_{p21} = \left(\frac{\overline{W}_{2+}}{\overline{W}_{1-}}\right)_{\overline{W}_{2-}=0}. \tag{2.45}$$

If we limit the study to the low and mid frequencies, that is where the three-dimensional waves inside the ATD are taken into account whereas only the plane waves are assumed to propagate at the inlet and outlet ports, then the source power as well as the sound power reflection and transmission coefficients can be derived using the plane wave methods. The time-averaged downstream and upstream propagating in-duct sound powers in the plane wave range can be written as

$$\overline{W}_{\pm} = \frac{|\tilde{p}_{\pm}|^2 S}{\rho_0 c_0}, \tag{2.46}$$

where $|\tilde{p}|$ is the RMS wave magnitude of the acoustic pressure, subscript $\pm$ denotes the downstream and upstream propagation, ρ_0 is the density, c_0 is the speed of sound and S is the cross-sectional area of the duct. Using Eqn. (2.46), Eqn. (2.44) becomes

$$S_{p11} = \left(\frac{|\hat{p}_{1+}|^2}{|\hat{p}_{1-}|^2}\right)_{\overline{W}_{2-}=0}. \tag{2.47}$$

Plugging the plane wave sound powers to Eqn. (2.45) leads to

$$S_{p21} = \left(\frac{Z_1}{Z_2} \frac{|\hat{p}_{2+}|^2}{|\hat{p}_{1-}|^2} \right)_{\overline{W}_{2-}=0}, \tag{2.48}$$

where Z is the characteristic impedance, $\rho_0 c_0/S$, at the inlet and outlet ports denoted with subscripts 1 and 2, respectively. Similarly, using $\overline{W}_{1-} = 0$, the corresponding sound power reflection and transmission coefficient can be derived, that is

$$S_{p22} = \left(\frac{|\hat{p}_{2+}|^2}{|\hat{p}_{2-}|^2} \right)_{\overline{W}_{1-}=0}, \tag{2.49}$$

and

$$S_{p12} = \left(\frac{Z_2}{Z_1} \frac{|\hat{p}_{1+}|^2}{|\hat{p}_{2-}|^2} \right)_{\overline{W}_{1-}=0}. \tag{2.50}$$

In Paper V [40], the elements of the power-scattering matrix are derived from the transmitted and reflected acoustic pressures using FEM. Note that, using the simulation model proposed, it is possible to determine the coefficients not only at the low and mid frequencies but also in the higher frequency range.

2.4 Two-ports for after-treatment devices with substrate

The acoustic performance of an ATD or filter can be evaluated using the transmission loss (TL) or insertion loss (IL), for example. Transmission loss is defined as the ratio of the incident to transmitted sound power assuming a reflection-free termination:

$$TL = 10log_{10}\left(\frac{\overline{W}_{incident}}{\overline{W}_{transmitted}} \right), \tag{2.51}$$

where $\overline{W}$ is the time-averaged sound power. When the total transfer matrix of the system is known, the transmission loss over the assembled system can be obtained straightforwardly using the transfer matrix elements as shown by Munjal [65]

$$TL = 10log_{10}\left\{ \frac{1}{4} \frac{Z_{out}}{Z_{in}} \left(\frac{1+M_{in}}{1+M_{out}} \right)^2 \left| T_{11} + \frac{T_{12}}{Z_{out}} + T_{21} Z_{in} + T_{22} \frac{Z_{in}}{Z_{out}} \right|^2 \right\}, \tag{2.52}$$

where Z is the characteristic impedance and $M = U/c$ is the Mach number, where U is the flow speed and c is the speed of sound. Note that Eqn. (2.52) is derived for plane waves but can directly be extended to the non-plane wave range using the power-based two-ports.

The most common way to describe the acoustic performance of a filter in practice is to use insertion loss. Insertion loss is defined as the ratio of the sound power at

the same point in the duct system for two different systems. That is, the insertion loss describes the change in the sound power level due to a system modification. To study the insertion loss of a filter, the radiated sound power from a straight empty duct is commonly used as the reference system:

$$IL = 10log_{10}\left(\frac{\overline{W}_{reference}}{\overline{W}_{system}}\right). \tag{2.53}$$

It can be noted that often for high frequencies the downstream reflections for systems with an open end are small and, therefore, the insertion loss will be equal to the transmission loss. The pressure and volume velocity are not continuous at a sudden area change at the inlet and outlet of the filter. The two-port model for the inlet and outlet ports is obtained using the principle of conservation of energy and momentum. When the Mach number is small, these relations can be derived assuming an incompressible mean flow. According to Allam and Åbom [7], these two-ports can be written as

$$\mathbf{T}_{in} = \begin{bmatrix} 1 & Z_{in}M_{in}(1/R_o^2 - 1) \\ 0 & 1 \end{bmatrix} \tag{2.54}$$

and

$$\mathbf{T}_{out} = \begin{bmatrix} 1 & 2Z_{out}M_{out}(1 - 1/R_o) \\ 0 & 1 \end{bmatrix}, \tag{2.55}$$

where R_o is the open area ratio.

The lumped resistance two-port model for the complete filter can be assembled using Eqn. (2.9) when the filter ("catalyser") two-port matrix $\mathbf{T}_{cat}$ is known

$$\mathbf{T}_{tot} = \mathbf{T}_{in}\mathbf{T}_{cat}\mathbf{T}_{out}. \tag{2.56}$$

In the following sections, two approaches to define the catalyser two-port matrix $\mathbf{T}_{cat}$ are proposed.

Motionless skeleton model

Damping in narrow channels can be taken into account with complex speed of sound, and density calculated according to the classic Kirchhoff solution [81, 56]

$$c_c = c_0\frac{\sqrt{1 - F(s)}}{\sqrt{1 + (\gamma - 1)F(\sigma s)}} \tag{2.57}$$

and

$$\rho_c = \frac{\rho_0}{1 - F(s)} \tag{2.58}$$

where c_0 is the adiabatic speed of sound, $\gamma = C_p/C_v$ is the ratio of the specific heat coefficient for constant pressure and constant volume, $\sigma^2 = \mu C_p/\kappa$ is the

Prandtl number, μ is the shear viscosity coefficient, κ is the gas thermal conductivity constant and

$$F(s) = \frac{2}{s\sqrt{-i}} \frac{J_1(s\sqrt{-i})}{J_0(s\sqrt{-i})} \tag{2.59}$$

where $s = r_c\sqrt{\rho_0\omega/\mu}$ is the Stokes number, r_c is the radius of the capillary, J_0 and J_1 are the zero and first order Bessel functions respectively. Eqns. (2.57) and (2.58) are valid for circular capillaries.

If the channel cross-sections are not circular, the radius r_c can be derived from the corresponding hydraulic diameter $r_c = D_{hyd}/2$. Using the complex density and speed of sound, the transfer matrix of a distributed catalyst element is written as

$$\mathbf{T}^I_{cat} = \begin{bmatrix} cos(k_{cat}L_{cat}) & iZ_{cat}sin(k_{cat}L_{cat}) \\ i/Z_{cat}sin(k_{cat}L_{cat}) & cos(k_{cat}L_{cat}) \end{bmatrix}, \tag{2.60}$$

where Z_{cat} is the characteristic impedance of the catalyst element, k_{cat} is the wave number and L_{cat} is the catalyst length. The characteristic impedance of the catalyst element is calculated by dividing the complex speed of sound and density, Eqns. (2.57) and (2.58), with the equivalent channel area of the catalyst

$$Z_{cat} = \frac{\rho_c c_c}{R_o S}, \tag{2.61}$$

where R_o is the open area ratio of the catalyst and S is the total frontal area. The catalyst wave number is $k_{cat} = \omega/c_c$. The channel length depends on the length of the element L and when the channels are formed using corrugated sheets, on the skew angle of the corrugations α

$$L_{channel} = \frac{L}{cos(\alpha)}. \tag{2.62}$$

For the uniform and unconnected channels as used in open foil-coated (OFC)-type catalysts [45], the catalyst length in Eqn. (2.60) equals the channel length, i.e. $L_{cat} = L_{channel}$. In the POC-X type filter, the wire mesh screens forms tortuous channels which are connected to each other. By introducing the X type particle oxidation catalyst (POC-X) wire mesh filter length correction factor ξ, the equivalent channel length can be defined

$$L_{eqv} = \xi L_{channel}. \tag{2.63}$$

In Paper V [40], the two-port for a selective catalytic reducer (SCR) filter is derived using FEM and the above-mentioned methods to take into account the damping in the substrate.

Finding the correction factors

In Paper VI [42] POC-X type filters are studied, the correction factor in Eqn. (2.63) is determined with unconstrained optimization and MATLAB® optimization toolbox. The target is to find the minimum of the objective function starting at an

initial estimate. The problem is specified as

$$\min_{\xi} |f(\xi)|, \tag{2.64}$$

where $f(\xi)$ returns a scalar value for the correction factor ξ. Only plane waves are propagating in the duct up to the cut-on frequency of the first non-plane wave mode. That is $f_{10,cut-on}$, where subscript 10 denotes the number of radial and circumferential nodal lines, respectively. In the plane wave frequency range, the simulation results can be compared with the transmission loss determined from the classic two-port measurements. The commonest way to describe the acoustic performance of a filter in the high frequency range with non-plane waves is the insertion loss. Therefore, the simulation results are compared to the insertion loss after the first non-plane wave mode cut-on frequency.

The target value is defined as the average difference over the samples and as the average difference in the 1/3 octave bands corresponding the plane wave or the non-plane wave frequency range. The piecewise objective function is then

$$f(\xi) = \begin{cases} \frac{1}{M}\sum_m \left(\frac{1}{N}\sum_n \left(\langle TL(\xi) \rangle_{1/3}^{calculated} - \langle TL \rangle_{1/3}^{measured} \right)_n \right)_m & , \\ f < f_{10,cut-on} & \\ \\ \frac{1}{M}\sum_m \left(\frac{1}{N}\sum_n \left(\langle TL(\xi) \rangle_{1/3}^{calculated} - \langle IL \rangle_{1/3}^{measured} \right)_n \right)_m & , \\ f \geq f_{10,cut-on}, & \end{cases} \tag{2.65}$$

where $\langle\ \rangle_{1/3}$ denotes summing in 1/3 octave bands, N is the number of samples and M is the number of 1/3 octave frequency bands in the corresponding plane wave and non-plane wave frequency ranges. The results of the optimization are the best fit wire mesh filter length correction factors.

The lumped resistance model

One way to estimate the acoustic two-port matrix of a filter is to neglect the frequency dependent wave propagation and treat the filter only as an acoustic resistance. This low frequency (plane wave) approach has been applied earlier by Allam and Åbom [5] to model the conventional DPF for frequencies where the filter length is smaller than the wavelength. Below, their formulation is revisited.

The continuity of the volume velocity over the resistive element holds, i.e. it does not change, but the pressure difference is proportional to the acoustic impedance of the filter times the output volume velocity. That is

$$\hat{q}_{in} = \hat{q}_{out} \tag{2.66}$$

and

$$\hat{p}_{in} - \hat{p}_{out} = \hat{q}_{out} Z_r, \tag{2.67}$$

where Z_r is the acoustic impedance, i.e. resistance (subscript r). Eqns. (2.66) and (2.67) can be written in the matrix form as

$$\begin{Bmatrix} \hat{p}_{in} \\ \hat{q}_{in} \end{Bmatrix} = \begin{bmatrix} 1 & Z_r \\ 0 & 1 \end{bmatrix} \begin{Bmatrix} \hat{p}_{out} \\ \hat{q}_{out} \end{Bmatrix}. \tag{2.68}$$

Assuming the steady flow pressure-drop to follow Darcy's law with Forchheimer's extension [30], it can be written as

$$\Delta p = R_l U + R_q U^2, \tag{2.69}$$

where Δp is the pressure drop, U is the flow velocity and R_l and R_q are the linear (subscript l) and quadratic (subscript q) flow resistance coefficients, respectively. Differentiating this yields to

$$\mathrm{d}\Delta p = \left(\frac{R_l + 2R_q U}{S} \right) \mathrm{d}US, \tag{2.70}$$

where S is the cross-sectional area of the filter and $\mathrm{d}US = \mathrm{d}q$ is the volume flow. Eqn. (2.70) implies that the acoustic resistance is

$$Z_r = \frac{R_l + 2R_q U}{S}. \tag{2.71}$$

Plugging Eqn. (2.71) into Eqn. (2.68), the lumped resistance acoustic two-port model for the filter is written as

$$\mathbf{T}_{cat}^{II} = \begin{bmatrix} 1 & (R_l + 2R_q U)/S \\ 0 & 1 \end{bmatrix}. \tag{2.72}$$

In Paper VI [42], damping of POC-X type filter is studied using the above-mentioned methods.

Chapter 3

Results and discussion

3.1 Experimental determination of the acoustic power weighting factors

In order to develop procedures for estimating the propagating sound power *in situ* for medium speed IC-engines a special rig was designed (Paper II). The idea was to allow measurements under controlled conditions and to investigate the effect of different source types and microphone configurations. The test-rig consists of a steel duct, loudspeakers, wall-mounted microphones, and a reverberation room. The test-rig is shown in Fig. 3.1. Total length of the duct assembly is 8500 mm, inner diameter of the duct is $\varnothing$=255 mm, and the wall thickness is 6 mm. In the earlier studies with the same steel duct, it was verified that, the duct is rigid enough to avoid the transmission noise through the wall as well as the noise caused by mechanical vibrations of the structure [73].

Monopole, dipole, and quadrupole source types are generated by phasing the array of four loudspeakers spaced equally around the circumference of the duct. Schematics of the loudspeaker array and the relative phases of the loudspeakers in monopole, dipole, and quadrupole source types are shown in Fig. 3.2. The four 10-inch loudspeakers used are of type Beyma 10MW/Nd. An ordinary audio amplifier was used to power the loudspeakers.

The sound pressures were measured from three cross-sections using four wall-mounted microphones in each cross-section spaced equally around the circumference. The cross-sections are located far enough from the source region that the near field phenomena can be neglected, see Fig. 3.1. The distances between the cross-sections were chosen to cover the plane wave range from 30 Hz to 810 Hz (c=340 m/s and air at 20°C), based on the two microphone method error analysis presented by Åbom and Bodén [3]. All the twelve 1/4 inch pressure field microphones are of type Brüel & Kjær 4935. The angle of rotation between the loudspeaker array and the three microphone cross-sections is approximately 10 degrees.

The closed end of the test duct was stuffed with polyester wool to achieve non-

Figure 3.1: Test-rig (orange pipe) for the high frequency acoustic power weighting factor determination. The absorbing end is to the left and the right-hand opening is connected to a reverberation room.

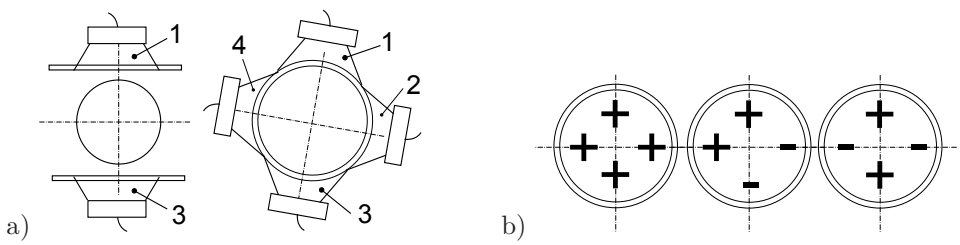

Figure 3.2: a) The loudspeaker setup for generating the monopole, dipole and quadrupole source types. b) Phasing of the four loudspeakers to generate acoustic source types, from left to right: monopole, dipole, and quadrupole.

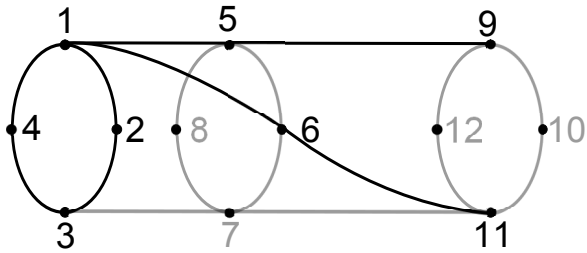

Figure 3.3: The microphone configurations used in the spectra averaging. 1-6-11 is the spiral microphone setup.

reflecting boundary condition. The other end of the test duct was attached to the 200 m^3 reverberation room to measure the produced sound powers of the different source types.

A total of three excitation cases were studied: monopole, dipole, and quadrupole. Sound power beyond the plane wave range was estimated using different wall-mounted microphone configurations and different averaging methods. The in-duct results were compared against sound power measured using the reverberation room method ISO 3741 [50].

Wide-band random noise excitation signal was used for all source types. The acoustic pressures from the duct were measured up to 12800 Hz at a frequency resolution of 0.25 Hz using a Hanning window with 50% overlap.

The experimentally derived 1/3 octave frequency band acoustic power weighting factors as a function of the 1/3 octave band Helmholtz number limits for monopole, dipole and quadrupole excitations are shown in Fig. 3.4. The results are given for the spiral microphone setup with cross-spectra averaging, see Fig. 3.3.

3.2 Acoustic power weighting factor simulations

As a continuation of the work in Paper II [39] a numerical study was undertaken in Paper IV [43]. The purpose of this was to systematically look for an optimum three-microphone configuration and to estimate the uncertainty.

Using simulations, the relative angular positions of the three microphones are varied to find the best microphone configuration. The high frequency in-duct sound power weighting factors $\varepsilon_{xy,1/3}$ are derived using Eqn. (2.43).

One metre of the test duct of $\varnothing$=255 mm was modelled using FEM. Note that, in order to make the results valid also for an arbitrary duct and temperature, they will be expressed relative to the Helmholtz number of the duct. The model of the test duct is shown in Fig. 3.5. The model consists of approximately 270 000 nodes and 1 300 000 elements. The three-dimensional tetrahedron elements were used to model the duct interior. The duct terminations were modelled as reflection-free

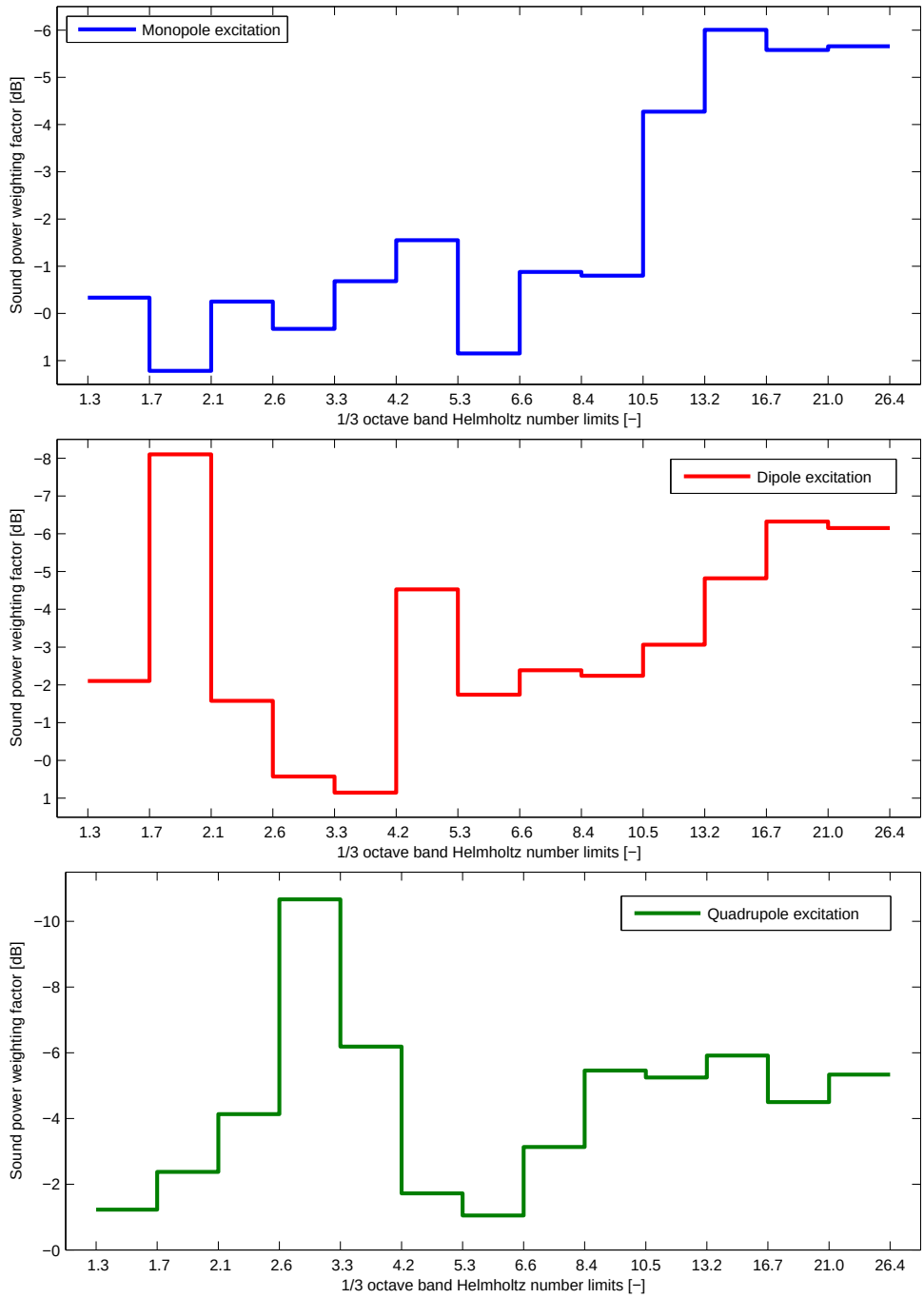

Figure 3.4: The experimentally derived 1/3 octave frequency band acoustic power weighting factors as a function of the 1/3 octave band Helmholtz number limits for monopole, dipole and quadrupole excitations.

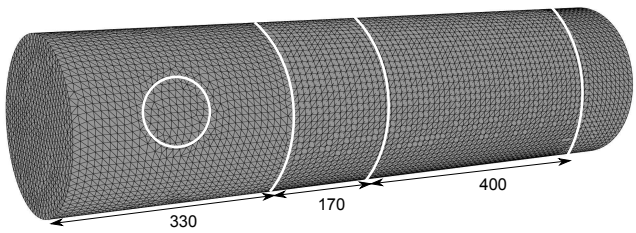

Figure 3.5: Finite element model of the one metre ⌀=255 mm test duct and the locations (mm) of the measurement cross-sections selected according to the low frequency plane wave decomposition criteria [3]. Both terminations are reflection-free, and this is modelled with infinite elements. The ⌀=100 mm circular region at the duct wall is the excitation area ("monopole").

ends using infinite elements. A typical element length was 5 mm. With the speed of sound of 340 m/s, this covers the frequency range up to the 1/3 octave band of centre frequency 6300 Hz ($He_c = 14.8$) when approximately ten elements per wavelength are required.

A steady state response was solved at a frequency range from 500 Hz to 8000 Hz using 1000 logarithmic steps, which leads to approximately 78 frequency points per 1/3 octave band. The ABAQUS 6.11 [1] software was used in the simulations.

The model was excited using the circular region of ⌀=100 mm at the duct wall. The circular area can be seen at the duct wall in Fig. 3.5. In order to excite all the modes, a complex volume acceleration (monopole source) corresponding to a pressure magnitude of 1 Pa was applied to the excitation region, that is $Q = pS/\rho c$. The damping is applied by defining a frequency-dependent flow resistance, i.e. volumetric drag in ABAQUS. This flow resistance is calculated from the viscous fluid losses, explained by Pierce [71], for example. At each frequency, the acoustic pressures at the nodes of the three circular cross-sections (shown in Fig. 3.5) were saved. In addition, the acoustic intensity over the duct cross-section near the end termination was saved.

First, by comparing the sound power integrated over the duct cross-section with the sound power derived using the acoustic pressures at the duct wall, the 1/3 octave frequency band acoustic power weighting factors $\varepsilon_{xy,1/3}$ are derived. In practice, to ensure that the turbulence pressure fluctuations are uncorrelated, the distance between the microphones must exceed the spatial integral scale of the turbulence field within the duct. According to gas turbine noise studies by Sacks et al. [74], a microphone distance of greater than 50% of the duct hydraulic diameter satisfies the correlation criteria. If the distance between the cross-sections is selected according

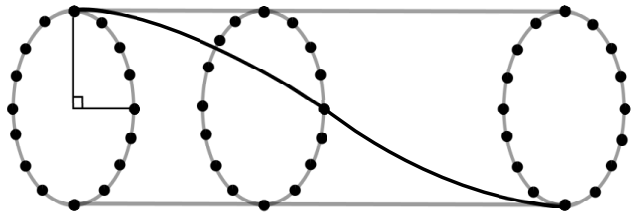

Figure 3.6: Acoustic pressure measurement points used to estimate the in-duct acoustic power. The distances between the sections are chosen to cover the plane wave range in the classic two-microphone measurements [3]. The spiral microphone configurations can be specified by defining the relative angular twist as the angle between the two neighbouring measurement points seen from the axial direction. From the microphone configurations studied, see Paper IV [43], the one with relative angular twist of 90° is shown with a solid black line.

to the low frequency measurements, e.g. [3], the criteria are automatically satisfied.

Second, to find the best three-microphone configuration, the acoustic power was derived using the three cross-sections shown in Fig. 3.5 with 16 measurement points each. The selected measurement points are shown in Fig. 3.6. The number of combinations to select the three measurement points from these is $16^3 = 4096$. Note that using that many microphone configurations, that is $3 \cdot 4096 = 12288$ cross-spectra, would be very time consuming in measurements. Taking that as the reference, five different three-microphone spiral configurations were studied. The spiral microphone configurations can be specified by defining the relative angular twist as the angle between the two neighbouring measurement points seen from the axial direction. The relative angular twists of these three-microphone configurations are 0° (i.e. axial, subscript ax), 22.5° (s1), 45° (s2), 90° (s3), 112.5° (s4). The three-microphone configuration with relative angular twist of 90° is shown in Fig. 3.6 with a solid black line.

To simulate the multi-modal excitation from a randomly located monopole, the relative angle between the monopole and the spirals is varied using steps of 22.5°. In that way, we get 16 cases for each of the microphone configurations.

Using the standard deviations of the five microphone configurations, the best three-microphone configuration is selected.

The sound pressure distribution was solved for each frequency. The sound pressure distribution at the frequency of 770 Hz is shown in Fig. 3.7 as an example. The excitation of the mode shape ψ_{10} ($f_{10,cut-on} \approx$788 Hz) can be noted from the sound pressure variation.

At each frequency step, the cross-spectra between the measurement points were averaged using Eqn. (2.42). The results were converted to 1/3 octave bands of centre frequencies of 630 Hz to 6300 Hz. In non-dimensional Helmholtz-scale the corresponding 1/3 octave band centre frequencies are $He_c = 1.5$ to $He_c = 14.8$.

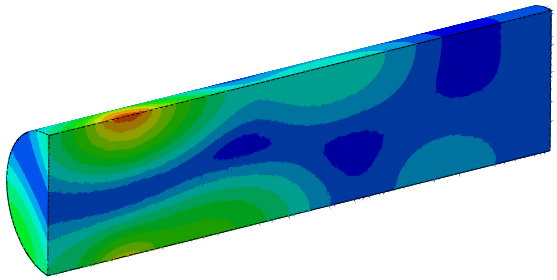

Figure 3.7: Sound pressure distribution at the frequency of 770 Hz. That corresponds to the Helmholtz frequency of 1.8. The colours in the figure describe magnitude of the sound pressure; ranging from higher sound pressure (red) to the lower sound pressure (blue). The excitation of the mode shape ψ_{10} ($f_{10,cut-on}$ ≈788 Hz) can be noted from the sound pressure variation.

Using this non-dimensional form, the results are usable at other speeds of sounds (i.e. temperatures) and duct sizes. For clarity, the piecewise sound power weighting factors are shown as a function of the limiting Helmholtz numbers. The simulated 1/3 octave frequency band acoustic power weighting factors are shown in Fig. 3.8. Also, the experimentally determined weighting factors for the monopole excitation from Paper II [39] are shown in Fig. 3.8. The simulated weighting factors with the corresponding standard deviations σ_{xy} are listed in Table 3.1 for the studied 1/3 octave bands, i.e. Helmholtz-scale center frequencies He_c. For clarity, also the lower and upper 1/3 octave band frequency limits He_l and He_u are listed in the table.

The standard deviations of the five studied three-microphone configurations (see Paper IV [43]) compared to the reference (all configurations, Table 3.1) are listed in Table 3.2. This means that, when one of these three-microphone configurations are used, the weighting factor is obtained from Table 3.1 and the total standard deviation is estimated as the sum of the values in Tables 3.1 and 3.2.

As can be seen from Fig. 3.8, the sound power weighting factor is approximately zero in the plane wave range. This is reasonable, since the plane wave in-duct acoustic mode shapes equals unity, i.e. there are no modal cross-terms. The experimentally determined weighting factor deviates from zero due to inaccuracies in the measurements. Note that the sound power weighting factors are used in Eqn. (2.43), which is only valid in the non-plane wave frequency range, that is $He_c > 1.5$. In the plane wave frequency range, the downstream and upstream propagating waves should be separated and the in-duct acoustic power derived using Eqn. (2.36). In the mid frequency range, there is some deviation as expected

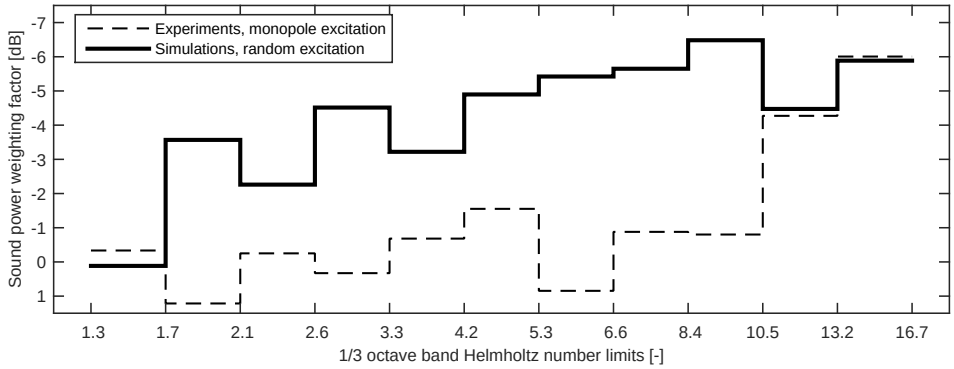

Figure 3.8: The 1/3 octave frequency band acoustic power weighting factors as a function of the 1/3 octave band limiting Helmholtz numbers. Solid line: Simulated weighting factors for multi-modal excitation based on 4096 microphone configurations, Paper IV [43]. Dashed line: Weighting factors for monopole excitation from experiments, Paper II [39].

Table 3.1: The 1/3 octave frequency band acoustic power weighting factors $\varepsilon_{xy,1/3}$ with standard deviations σ_{xy} based on 4096 microphone combinations.

He_l	He_c	He_u	$\varepsilon_{xy,1/3}$	σ_{xy}
	(-)		(dB)	
1.3	1.5	1.7	0.1	0.0
1.7	1.9	2.1	-3.6	4.1
2.1	2.4	2.6	-2.3	4.1
2.6	2.9	3.3	-4.5	2.9
3.3	3.8	4.2	-3.2	1.6
4.2	4.7	5.3	-4.9	2.6
5.3	5.9	6.6	-5.4	2.5
6.6	7.4	8.4	-5.6	0.9
8.4	9.4	10.5	-6.5	1.0
10.5	11.8	13.2	-4.5	0.7
13.2	14.8	16.7	-5.9	0.6
maximum				4.1
average				2.0

Table 3.2: The standard deviations of the five studied three-microphone configurations. The result derived using all 4096 microphone combinations was used as the reference (Table 3.1).

He_l	He_c	He_u	σ_{ax}	σ_{s1}	σ_{s2}	σ_{s3}	σ_{s4}
(-)			(dB)				
1.3	1.5	1.7	0.8	1.0	1.1	1.2	1.3
1.7	1.9	2.1	3.2	1.5	3.1	3.3	2.9
2.1	2.4	2.6	2.5	1.5	2.6	3.1	3.3
2.6	2.9	3.3	2.7	2.2	2.8	2.1	2.7
3.3	3.8	4.2	1.1	1.0	0.9	0.8	1.4
4.2	4.7	5.3	3.3	2.4	1.9	3.1	3.6
5.3	5.9	6.6	2.6	1.9	2.9	2.8	2.2
6.6	7.4	8.4	1.1	1.0	0.8	0.8	1.1
8.4	9.4	10.5	1.3	1.0	1.4	1.4	0.9
10.5	11.8	13.2	1.0	0.9	1.4	1.3	0.9
13.2	14.8	16.7	0.9	0.8	1.1	1.0	1.1
maximum			3.3	2.4	3.1	3.3	3.6
average			1.9	1.3	1.8	1.9	1.9

between the experimental and simulated data. This is, of course, due to the fact that the experiments are carried out for a certain monopole configuration, while the simulations are an average over a number of configurations.

At higher frequencies, the sound power weighting factors derived with the cross-spectra are converging to -6 dB value. As can be noted from Fig. 3.8, a similar trend was achieved experimentally in Paper II [39]. The sound pressure at the duct wall is related to the sound pressure averaged over the cross-section. According to Joseph et al. [54], theoretically this relationship tends to two, that is 3 dB. In the semi-diffuse field, the acoustic energy at a point in the duct arrives equally from all angles over a hemi-sphere. This also leads to a power weighting of 3 dB. In that sense, the convergence to the value of 6 dB is reasonable.

From the standard deviations of the five microphone configurations studied that are listed in Table 3.2 it can be concluded that the spiral with 22.5° relative angular twist has the lowest average value, 1.3 dB, as well as the lowest maximum value of 2.4 dB. The average values of the other microphone configurations are equal or more than 1.8 dB, and the maximum values are at least 3.1 dB. The sound pressure at the duct wall depends strongly on the circumferential position of the microphones. When using the spirals with the relative angular twist of 45° or 90°, the deviation is strongest when the first non-plane wave acoustic mode starts to propagate, i.e. the 1/3 octave frequency band $He_c = 1.9$. The spiral with the relative angular twist of 112.5° catches the mode Ψ_{30} (see Table 2.1) causing the maximum standard deviation of 3.6 dB at the corresponding 1/3 octave frequency band. Therefore, it

can be concluded that the best three-microphone configuration found in this study is the spiral with the lowest relative angular twist, that is 22.5°.

As a conclusion, it can be said that, when the excitation is not exactly known, it can be assumed to be multi-modal, i.e. exciting all possible in-duct modes. In that case, the high frequency in-duct acoustic power can be estimated using the new formulation explained in detail in Paper IV [43] and summarized here. See Eqn. (2.43) with the numerical estimates for the 1/3 octave frequency band weighting factors $\varepsilon_{xy,1/3}$ listed in Table 3.1.

Using the non-dimensional Helmholtz-scale form, the results are usable for other speeds of sounds (i.e. temperatures) and duct sizes. In this study, the phenomena were simulated up to the frequency of $He = 16.7$ due to limitations of the computational resources. In the higher 1/3 octave frequency bands, $He_c > 14.8$, the asymptotic value of $\varepsilon_{xy,1/3}$ =-6 dB should be used. According to this study, it is recommended to measure the cross-spectra S_{xy} in Eqn. (2.43) using three-microphones with relative angular twist of 22.5°. The same microphone configuration can then be used to measure the low frequency plane wave range in-duct acoustic power, if the distances between the measurement cross-sections are selected correctly, according to [3] for example.

3.3 Acoustic source characteristics of medium speed IC-engine exhaust noise

The test engine studied (Papers I and III) is a four-stroke four-cylinder inline engine of type Wärtsilä Vasa 4R32. The engine operates at a constant speed of 750 rpm, producing 1640 kW of power. The cylinder bore is 320 mm, and the stroke is 350 mm. The engine weighs 20.3 tons. The turbine of the turbocharger of type BBC VTR 254 has 45 blades and the nominal rotation speed is 30 000 rpm. The test engine shown in Fig. 3.9 is located in the VTT engine laboratory in Otaniemi, Espoo, Finland. The static pressure, temperature, the mass flow rate of the exhaust gas and the engine and turbocharger rotation speeds were measured. The pressure transducers were type WCT-312M-25A produced by Kulite, and they were connected to a water cooling circuit. The mass flow rate was measured with an ISA 1932 nozzle system.

As validated in Paper I [46], the low frequency plane wave source data can, for medium speed IC-engines, be obtained from simulations using one-dimensional process simulation software. The low frequency plane wave range acoustic source characteristics of the test engine were obtained by simulating the acoustic multi-load method measurements. GT-Power software [34] was used to solve the nonlinear set of partial differential equations describing the gas dynamics of the test engine. The simulation model of the test engine was validated with engine performance and cylinder pressure measurements.

In Paper III [41], the cut-on frequency of the first non-plane wave mode ψ_{10} was also measured using the method proposed in Paper II [39]. The phase shifts

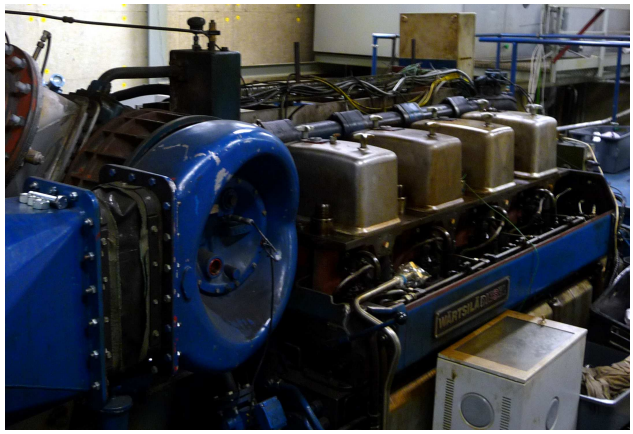

Figure 3.9: The test engine, Wärtsilä Vasa 4R32 in the VTT engine laboratory.

of the measured transfer functions between the opposite microphones, i.e. one-three and two-four in [46], are shown in Fig. 3.10. To estimate the high frequency non-plane wave range source characteristics of the diesel engine studied on the exhaust side, the acoustic pressure was measured using six measurement points in the exhaust duct. The pressures were measured from three sections. Four wall-mounted pressure transducers were used in the first measurement section in the circumferential configuration, and the transducers were evenly mounted around the circumference, see Fig. 3.11. One pressure transducer was used in each of the two other sections. Originally, the distances between the measurement sections were defined for the low frequency plane wave range measurements according to the method proposed by Åbom and Bodén [3].

The simulated, plane wave frequency range source sound powers combined with the measured non-plane wave source data are shown in 1/3 octave frequency bands in Fig. 3.12. The axial configuration was used in the measured source data with the random source type sound power weighting factors shown in Fig. 3.8. For clarity, the source sound power is A-weighted. Note that weighting was not used in Paper III [41].

One aim of this study was to investigate how to combine the source characteristics in the low frequency plane wave range with those of the high frequency non-plane wave range for multi-port simulations. Using the suggested sound power-based formulation to describe the outgoing source power, the source characteristics of an IC-engine exhaust system can be combined in a way that preserves the mathematical structure of two-port matrix formalism. This is important since it opens the possibility also to extend two-port simulation softwares to include the high frequency range.

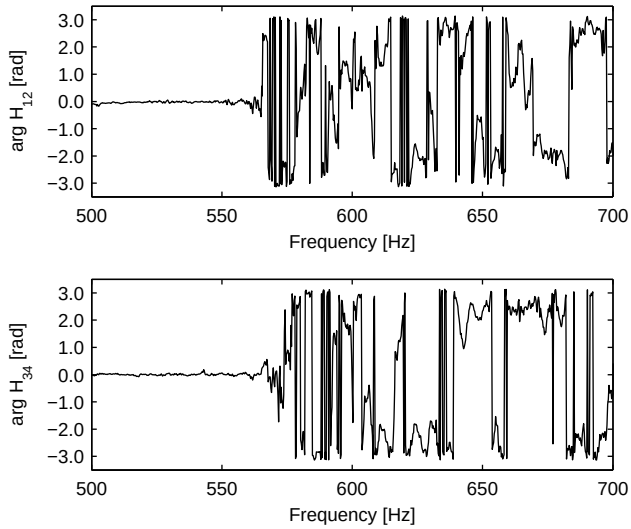

Figure 3.10: The measured phase shift between the opposite microphones, one-three above and two-four below. The phase of microphones one-three and two-four turns from in phase to out phase ($arg(H) \approx \pi$ rad) at frequencies of 568.5 Hz and 578.3 Hz respectively. Using these measured cut-on frequencies, the speed of sound can be determined, see Paper III [41].

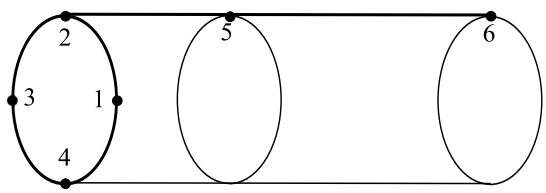

Figure 3.11: Pressure transducer configuration used in the exhaust pipe after the turbocharger. The axial and circumferential configurations consist of transducers 2-5-6 and 1-2-3-4 respectively, see Paper III [41].

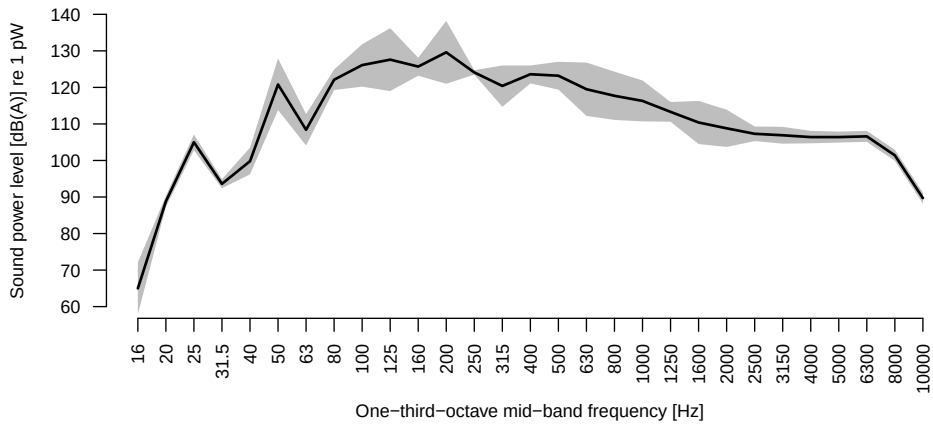

Figure 3.12: The combined low and high frequency A-weighted source sound power level of the test engine exhaust noise in 1/3 octave frequency bands. The shaded area describes the reliability of the method. In the plane wave frequency range, the reliability is estimated by comparing the simulations with measurements, see Paper I [46]. Beyond the plane wave range, the reliability is estimated using standard deviations shown in Paper IV [43] and in Tables 3.1 and 3.2 for the weighting factors and axial microphone configuration, respectively.

It can be noted from Fig. 3.12 (and from Papers I and III [46, 41]), that most of the acoustic energy is in the low frequency plane wave range. There are strong peaks at the 1/3 octave bands of frequencies 25 Hz and 50 Hz. These are exactly at the first two engine cycle harmonics, i.e. the second and fourth crankshaft rotation order. It can be noted that, in general, the high frequency source power is much lower than the low frequency source power.

3.4 Determination of the the low and mid-frequency range noise attenuation of medium speed IC-engine after-treatment device

In Paper V [40] the three-dimensional wave propagation inside the ATD is simulated with FEM. The interaction between the flow and acoustic field is neglected. The complex substrate material properties are calculated with the Kirchhoff solution, using the hydraulic diameter of the capillaries. New methods for the effective sub-

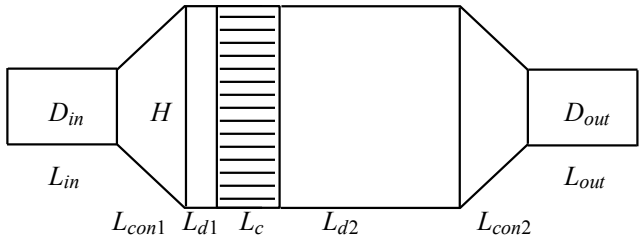

Figure 3.13: Schematic of the tested after-treatment device (see Paper V [40]). The main dimensions and the substrate (hatched area) properties are listed in Tables 3.3 and 3.4, respectively.

Table 3.3: The main dimensions of the tested after-treatment device

$D_{in,out}$ (mm)	H (mm)	$L_{in,out}$ (mm)	L_{d1} (mm)	L_{d2} (mm)	L_c (mm)	$L_{con1,2}$ (mm)
1100	2330	1000	333	4678	200	800

Table 3.4: The properties of the substrate

D_{hyd} (mm)	cell density (cpsi)
2.7	64

strate modelling are sought. In addition, procedures to extend the one-dimensional two-ports into the higher frequencies are proposed. The noise attenuation of a test ATD is estimated at the low and mid-frequency range and the results are compared with the measurements.

Schematic of the tested ATD is shown in Fig. 3.13. The main dimensions and the substrate properties are listed in Tables 3.3 and 3.4. The gas properties (air at 20 °C) are listed in Table 3.5.

The insertion losses from the analytical and FEM calculations as well as from the measurements are shown in Fig. 3.14 as a function of the dimensionless frequency, i.e

Table 3.5: The properties of the air at 20 °C during the tests with no flow.

T (°C)	ρ_0 (kg/m^3)	C_p (kJ/(kg K))	$\mu \times 10^5$ (Pa s)	$\kappa \times 10^2$ (W/(m K))	γ (-)
20	1.19	1.01	1.82	2.58	1.4

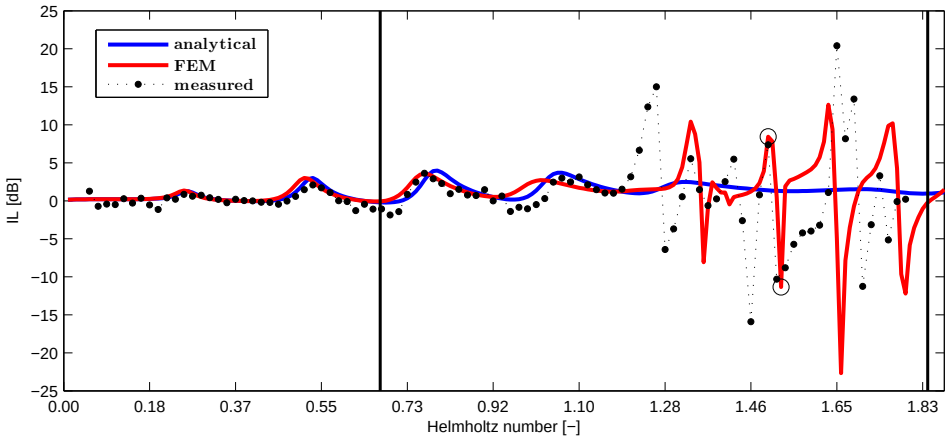

Figure 3.14: The analytical, FEM and measured insertion loss of the test ATD as a function of the Helmholtz number, from Paper V [40]. The cut-on frequency of the first non-plane wave mode in the chamber is denoted with the first thick vertical line. The second thick vertical line denotes the cut-on frequency of the first non-plane wave mode in the inlet duct.

Helmholtz number $He = kR$, where k is the wave number and R is the radius of the inlet and outlet ducts. The cut-on frequency of the first non-plane wave mode in the ATD chamber is denoted with the first thick vertical line. The second thick vertical line denotes the cut-on frequency of the first non-plane wave mode in the inlet and outlet ducts. To clarify the the three-dimensional acoustic wave propagation in the ATD, the sound pressure magnitude distribution at the frequencies of $He = 1.50$ and $He = 1.53$ for 1 Pa excitation at the inlet are shown as contour plots in Figs. 3.15 and 3.16, respectively. The corresponding peaks are marked with circles in the insertion loss curve in Fig. 3.14.

It can be seen from Fig. 3.14, that the analytical, FEM and measured results are almost equivalent up to the first cut-on frequency of the ATD chamber denoted with the first thick vertical line. From that frequency up to the cut-on frequency of the inlet and outlet ducts, i.e. the second vertical line Fig. 3.14, the analytical results are strongly deviating from the FEM and measured insertion losses. As can be noted in the measurements and FEM results, the insertion loss amplitude is oscillating at the frequency range between the cut-on frequencies shown, i.e. mid frequencies. At the positive peaks, the sound power reflections are strong whereas at the negative peaks the sound power runs through the ATD rather freely. This phenomenon is also visible in Figs. 3.15 and 3.16. The test ATD is assembled from subelements which are welded or bolted together. The joints and the stiffeners inside the ATD are neglected in the FEM model. In addition, the insertion loss

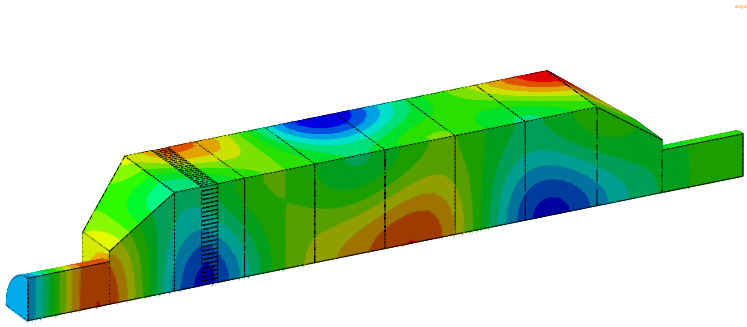

Figure 3.15: Acoustic pressure distribution of the tested ATD at the frequency of $He = 1.50$ for 1 Pa excitation at the inlet (left end). The sound reflections in the ATD are strong, which can be seen as weak wave propagation at the outlet duct. From Paper V [40].

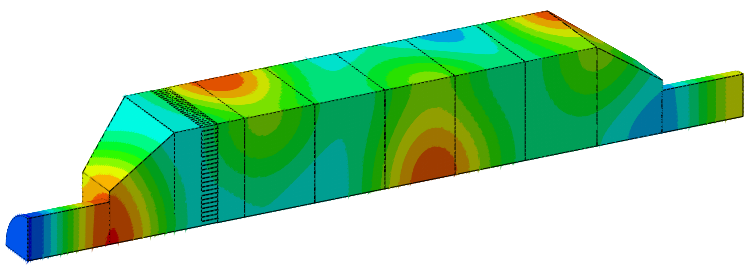

Figure 3.16: Acoustic pressure distribution of the tested ATD at the frequency of $He = 1.53$ for 1 Pa excitation at the inlet (left end). The sound transmission trough the ATD is strong, which can be seen as propagating waves at the outlet duct. From Paper V [40].

was not measured in optimal conditions, and the disturbing noise sources were not completely eliminated. Due to these inaccuracies, the FEM results does not exactly match with the measured ones, but it can be concluded that the general three-dimensional behaviour in the mid frequency range is estimated rather well.

The FEM model reduction based on modelling only a few channels seems to work as expected. The acoustic pressure distribution through the channels is assumed to be plane waves, which can be noted at the substrates in Figs. 3.15 and 3.16. Using the classic Kirchhoff solution with the hydraulic radius of the channels to determine the complex material properties of the substrate is an effective way to model the sound attenuation of the ATD. Using these modelling techniques, the substrate model can be reduced considerably while catching the correct acoustic behaviour.

In this study, the sound power reflection and transmission coefficients, i.e. the elements of the power-scattering matrix were derived using FEM. In the low and mid frequency range, the power coefficients can be derived straightforwardly from the sound pressures of the propagating plane waves at the inlet and outlet ducts of the ATD. In the higher frequency range, where the in-duct wave propagation is more complicated, the sound power can be determined via intensity integration. The power-scattering matrix can be measured using standardized methods, e.g., [51]. Unfortunately in practice the harsh environment prevents the use of the standardized methods and the measurements of the ATD must be conducted *in situ*. One alternative is to use wall-mounted microphones and the in-duct sound power measurement methods proposed in Papers II and IV [39, 43].

It can be concluded that, using the method shown here and in Paper V [40], the three-dimensional wave propagation in the test ATD can be taken into account in two-port simulations in the low and mid frequencies. This is of great importance when the acoustically optimal substrate configuration is sought. With the method shown, the study can also be extended into the high frequency range, i.e. where the non-plane waves propagate at the inlet and outlet ducts.

3.5 Two-ports for the particle oxidation catalyst POC®

Conventional DPF requires regular active regeneration and periodic ash removal to operate. Alternative after-treatment solutions have been developed to avoid these costly maintenance procedures. One of these is the X type particle oxidation catalyst, POC-X [60, 61, 57, 37]. The structure of the POC-X substrate forms tortuous channels running through the filter allowing the exhaust gas to either flow through the substrate cells formed from the metallic wire mesh screens or along the tortuous channels in the case of overloaded or blocked substrate (see Fig. 3.17).

The procedure explained in the Theory section 2.4 was applied to experimental data determined from four POC-X type filters in Paper VI [42]. Data of the tested filters is shown in Table 3.6. The diameter of the tested filters is $\varnothing = 200$ mm.

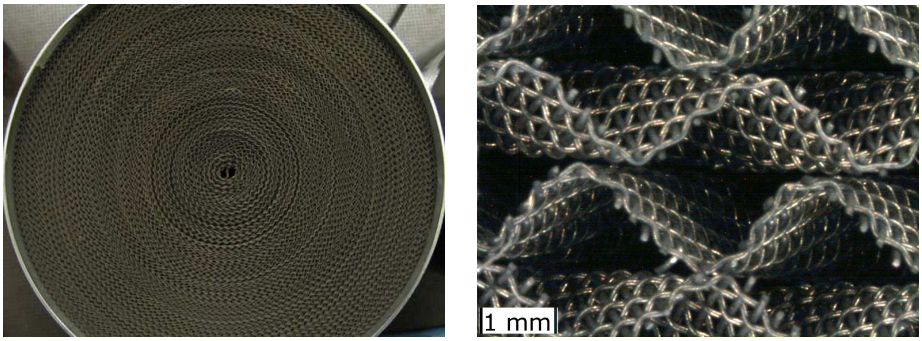

Figure 3.17: POC-X type filter (left) and microscope photograph of the substrate cells formed from the metallic wire mesh screens (right), see Paper VI [42].

Table 3.6: Data for the tested POC-X samples. Cell density unit, cpsi, means cells per square inch, R_o is the open area ratio, R_l and R_q are the linear and quadratic flow resistance coefficients determined experimentally.

cell density (cpsi)	L (mm)	α (deg)	D_{hyd} (mm)	R_o (%)	R_l (Ns/m^4)	R_q (Ns^2/m^5)
400	120	34	1.23	0.69	1270.7	426.8
200	120	20	1.96	0.79	247.6	147.0
300	180	34	1.51	0.74	721.3	362.9
300	100	34	1.51	0.74	918.9	407.4

The transmission loss of the filters was determined from the measured two-port data in the 1/3 octave frequency bands from centre frequency of 25 Hz to 800 Hz using the scattering matrix method [2]. The insertion loss was measured using a standardized method [52] up to the 1/3 octave band with centre frequency of 8000 Hz.

The transfer matrices of the filters were determined according to Sec. 2.4 and the transmission loss was determined using Eqn. (2.52). The gas properties (air at 20 °C) used in the simulations are listed in Table 3.5.

In the following, the results using the motionless skeleton model $\mathbf{T}_{cat}^{I}$, Eqn. (2.60), and using the lumped resistance model $\mathbf{T}_{cat}^{II}$, Eqn. (2.72), are shown and compared with measurements.

The correction factors for the motionless skeleton model were determined with the MATLAB® optimization tool-box and Eqns. (2.64) and (2.65). Number of samples $N = 4$ in Eqn. (2.65), and the number of 1/3 octave frequency bands $M = 16$ in the plane wave frequency range and $M = 11$ in the non-plane wave frequency range. As a result, the best fit wire mesh filter length correction factors

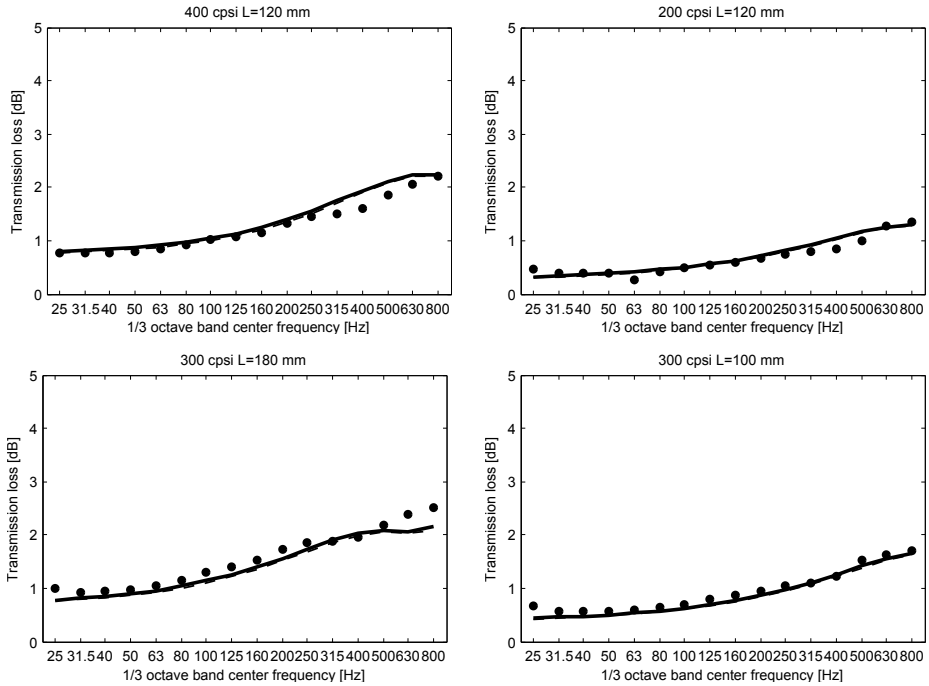

Figure 3.18: The simulated (lines) and measured (marks) transmission losses of the tested filters in the plane wave frequency range. The uncorrected simulation results (with the correction factor of $\xi = 1.00$) are plotted with dashed lines and results with the correction factor of $\xi = 1.03$ with solid lines. From Paper VI [42].

were found

$$\xi = \begin{cases} 1.03 & , f < f_{10,cut-on} \\ 1.48 & , f \geq f_{10,cut-on}. \end{cases} \tag{3.1}$$

The simulated and measured transmission losses and insertion losses for the motionless skeleton model are shown in Figs. 3.18 and 3.19, respectively. For comparison, the uncorrected simulation results ($\xi = 1.00$) are also shown.

The flow resistance coefficients R_l and R_q were calculated from the measured pressure drops using least squares [45]. The flow resistance coefficients are listed in Table 3.6. The measured and simulated attenuation in 1/3 octave frequency bands in the plane wave frequency range with M=0.01 for the lumped resistance model are shown in Fig. 3.20.

It can be noted from the upper sub figures in Figs. 3.18 and 3.19 that the attenuation increases with the channel density, cpsi. It is also clearly visible in the lower sub figures that the attenuation increases with the filter length, which is

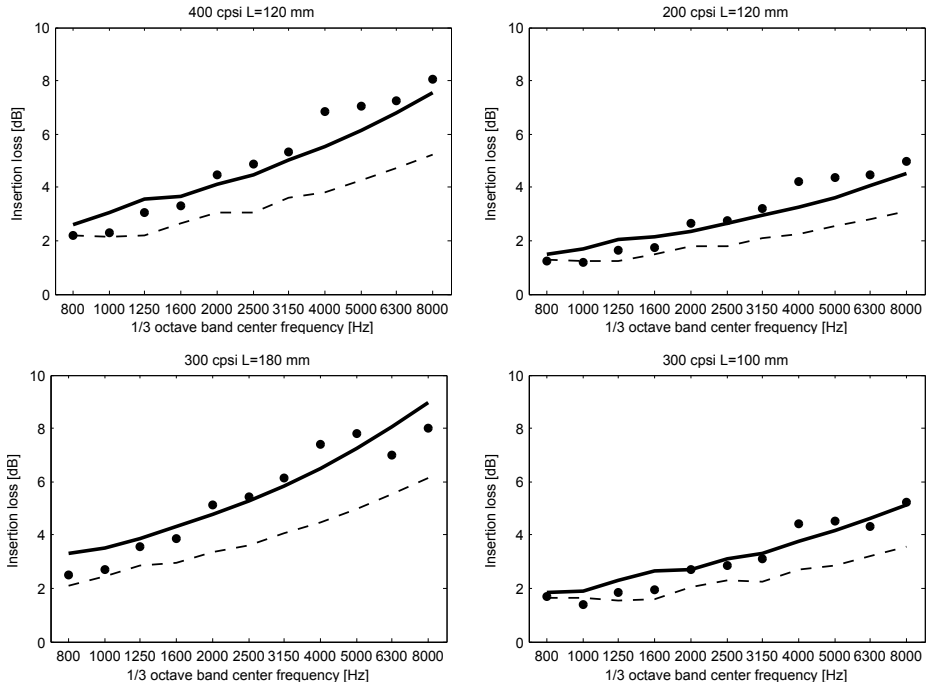

Figure 3.19: The simulated (lines) and measured (marks) insertion losses of the tested filters in the non-plane wave frequency range. The uncorrected simulation results (with the correction factor of $\xi = 1.00$) are plotted with dashed lines and results with the correction factor of $\xi = 1.48$ with solid lines. From Paper VI [42].

intuitively correct.

The best fit correction factor in the plane wave frequency range is 1.03, which means that the filter length used in the classic Kirchhoff solution with uniform channels must be increased only by 3%. It can be noted that the dashed and solid lines in Fig. 3.18 are on top of each other. Based on that, the frequency dependent, low frequency, plane wave frequency range acoustic behaviour of POC-X filter can be simulated with reasonable accuracy assuming unconnected, uniform channels, i.e. $\xi = 1.00$.

The corresponding filter length increase in the non-plane wave frequency range is 48% compared to the basic Kirchhoff solution. As can be noted from Fig. 3.19, the simulated results with the correction factor of $\xi = 1.48$ fit with the measurements quite well. In the investigated high frequency range, the deviation between the simulated results using the proposen correction factors, and the measurements is approximately within 1 dB. Compared to the uncorrected results plotted with dashed lines the improvement is significant.

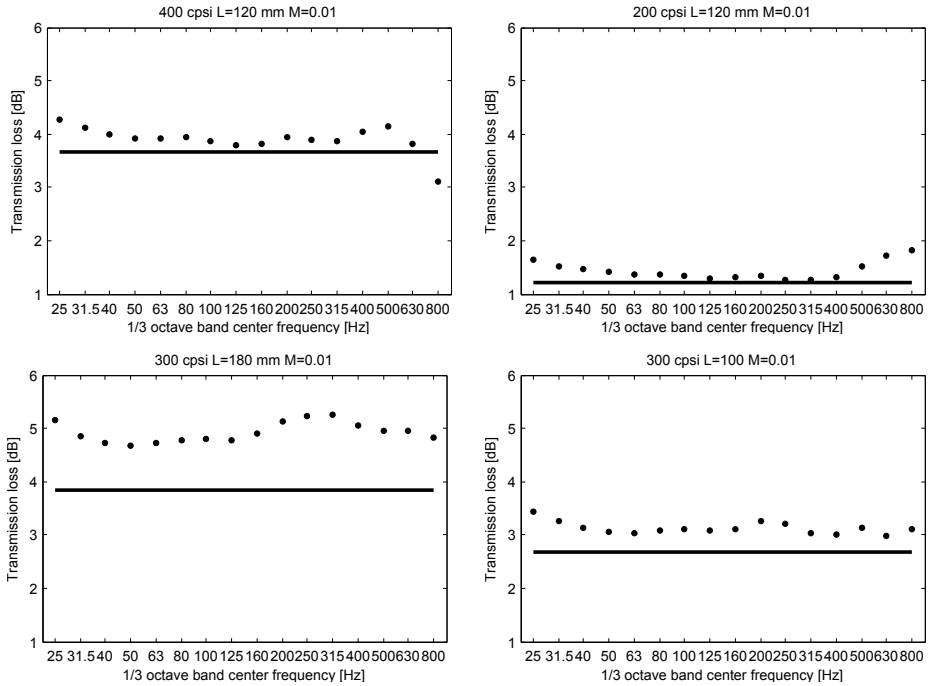

Figure 3.20: The simulated (lines) and measured (marks) transmission losses of the tested filters in the plane wave frequency range with M=0.01. From Paper VI [42].

Again, it can be noted from the results with flow, upper sub figures in Fig. 3.20, that the attenuation increases with the channel density, and from the lower sub figures that the attenuation increases with the filter length. In general, it can be said that the lumped resistance simulation model estimates the overall TL in the low frequency range quite well, being slightly conservative. Compared to the measured values, the deviation is approximately within 1 dB.

It should be noted that, instead of fitting each simulation model to the corresponding measurement data, the best fitting equivalent filter length was determined in the plane wave and non-plane wave frequency range for the set of samples. Data fitting based on experiments is necessary when a detailed simulation model of the filter is not readily available. To gain a deep understanding of the three-dimensional effects in the substrate, detailed data of the filter construction, i.e. wire mesh geometry, porosity parameters, etc. must be considered.

Chapter 4

Conclusions and future work

This thesis investigates the acoustic in-duct source characterization of fluid machines with applications to medium speed IC-engines. The plane wave source characterization methods are extended into the higher frequency range with non-plane waves using sound power-based approach. The in-duct sound power is estimated using the sound power weighting factors. In this thesis, the factors are defined for measurements conducted using the cross-spectra of wall-mounted microphones at three cross-sections of the duct.

The high frequency, non-plane wave range acoustic source characterization is of great importance when designing the duct systems with relatively large diameters, e.g. compressors, pumps and medium speed IC-engines. The sound power-based two-ports with the source terms shown in this thesis is an easy and computationally effective method to solve the sound propagation in a complete duct system including source, transmission path and receiver. This is very useful when optimizing the noise emission from a cruise ship or power plant, for example.

In addition, new acoustic models for the non-plane wave range are proposed and investigated for different after-treatment devices. Since such devices are now a standard also for medium speed IC-engines in many regions, this is an important contribution.

4.1 Acoustic source characterization

According to this thesis and Papers I, II, III and IV [46, 39, 41, 43], the best strategy for analysing the noise radiation from a medium speed IC-engine exhaust system is to use a one-port source model together with two-port based transmission path elements. In the plane wave range, the one-port source can be obtained from simulations, and the noise radiation can be solved in selected frequencies or in frequency bands. In the non-plane wave range, using the power-based formalism based on an estimate of the engine in-duct sound power under reflection-free conditions is recommended. This combined approach is important since the power-based formalism

normally suggested for larger ducts in standards and handbooks, must be used with care for medium speed IC-engines with very strong low frequency harmonics. For such systems, the plane wave range must be analysed using a wave-based approach, and the power-based model only applied above the cut-on frequency. It was shown that the measured high frequency source sound power combines smoothly with the simulated, low frequency source data; see Fig. 3.12.

To summarize the source characterization, according to this study the best microphone configuration is obtained by selecting the distances s between the three measurement cross-sections using $0.1\pi < ks < 0.8\pi$ [3] and using angular twist of $\pi/4$ in the spiral microphone configuration, see Paper IV [43]. Using the proposed procedure, the in-duct sound power beyond the plane wave range, can be estimated with an average standard deviation of approximately 3 dB in each 1/3 octave band, see Tables 3.1 and 3.2.

4.2 Acoustic damping for after-treatment devices

Using the approach shown in Papers V and VI [40, 42], the classic plane wave frequency range Kirchhoff solution for prediction of the acoustic wave attenuation in narrow channels is extended to the non-plane wave frequency range. Once the ATD data has been determined for cold conditions, predictions for hot conditions can be made by scaling the model parameters, e.g. adiabatic speed of sound, density, viscosity and thermal conductivity. The acoustic behaviour of POC-X type filters shown in Paper VI [42] was studied further in [44], where a procedure to estimate the acoustic behaviour of the filters with moderate Mach-numbers in the non-plane wave frequency range was introduced.

4.3 Future work

A natural continuation of this work is to validate the source characterization methods shown with a complete medium speed IC-engine exhaust system, for example. Due to large dimensions of the exhaust pipe ($\varnothing \geq$ 1 m), the acoustic loads for the source characterization measurements must be selected carefully. This process must be optimized with simulations. Another challenge is to conduct the three-microphone measurements *in situ* in a harsh environment. A complete simulation model of an IC-engine and the exhaust system should be built for validation purposes. For the high frequency non-plane wave range, defining the sound power two-ports for all of the transmission elements such as different types of turbochargers, boilers, after-treatment devices and silencers is demanding.

The suggested methods for in-duct sound power determination should be applied to perform full scale after-treatment device measurements. The major challenge here too is the *in situ* measurements. The acoustic behaviour of after-treatment device such as POC-X type filter is a multi-physical problem. Simulating the acous-

tic behaviour of POC-X might require computationally expensive fluid-structure-acoustic interaction model.

Finally, the complete medium speed IC-engine exhaust system with source, after-treatment devices and silencers should be optimized with simulation models for the most suitable noise reduction solution. Of course, the best option would be the compact, easily manufacturable singe emission eliminator for noise and air pollution.

It is also to be investigated how the methods proposed in this thesis are applied to study the acoustic behaviour of other fluid machines than IC-engines, e.g. pumps, compressors and fans.

Bibliography

[1] ABAQUS. Abaqus 6.11 analysis user's manual. *Simulia Dassault Systèmes*, 2011.

[2] M. Åbom. Measurement of the scattering-matrix of acoustical two-ports. *Mechanical Systems and Signal Processing*, 5(2):89–104, 1991.

[3] M. Åbom and H. Bodén. Error analysis of two-microphone measurements in ducts with flow. *The Journal of the Acoustical Society of America*, 83:2429, 1988.

[4] F. Albertson, H. Bodén, and J. Gilbert. Comparison of different methods to couple nonlinear source descriptions in the time domain to linear system descriptions in the frequency domain–application to a simple valveless one-cylinder cold engine. *Journal of Sound and Vibration*, 291(3-5):963–985, 2006.

[5] S. Allam and M. Åbom. Acoustic modelling and testing of diesel particulate filters. *Journal of Sound and Vibration*, 288(1):255–273, 2005.

[6] S. Allam and M. Åbom. Investigation of damping and radiation using full plane wave decomposition in ducts. *Journal of Sound and Vibration*, 292(3-5): 519–534, 2006.

[7] S. Allam and M. Åbom. Modeling and testing of after-treatment devices. *Journal of Vibration and Acoustics*, 128(3):347–356, 2006.

[8] S. Allam and M. Åbom. Sound propagation in an array of narrow porous channels with application to diesel particulate filters. *Journal of Sound and Vibration*, 291(3):882–901, 2006.

[9] F. Arnold. Experimentelle und numerische untersuchung zur schalleistungsbestimmung in strömungskanälen. In *VDI-Fortschritt-Berichte Reihe 7 Strömungstechnik No 353.* 1999.

[10] R.J. Astley and A. Cummings. Wave propagation in catalytic converters: Formulation of the problem and finite element to solution scheme. *Journal of Sound and Vibration*, 188(5):635–657, 1995.

[11] L. Backlund and P. Sundström. Compact silencer system - for reduced noise. *Wärtsilä technical journal*, (2):53–55, 2008.

[12] H. Bodén. On multi-load methods for determination of the source data of acoustic one-port sources. *Journal of Sound and Vibration*, 180(5):725–743, 1995.

[13] H. Bodén. One-sided multi-port techniques for characterisation of in-duct samples with nonlinear acoustic properties. *Journal of Sound and Vibration*, 331(13):3050–3067, 2012.

[14] H. Bodén. Two-sided multi-port techniques for characterisation of in-duct samples with non-linear acoustic properties. *Acta Acustica united with Acustica*, 99(3):359–378, 2013.

[15] H. Bodén and F. Albertson. In-duct acoustic one-port sources, linear or non-linear. *INTERNOISE*, 1:227–230, 1998.

[16] H. Bodén and R. Glav. Exhaust and intake noise and acoustical design of mufflers and silencers. In M.J. Crocker, editor, *Handbook of noise and vibration control*, chapter 85. Wiley, 2007.

[17] H. Bodén and M. Åbom. Modelling of fluid machines as sources of sound in duct and pipe systems. *Acta Acustica*, 3:549–560, 1995.

[18] H. Bodén, M. Tonsa, and R. Fairbrother. On extraction of IC-engine linear acoustic source data from non-linear simulations. *Proceedings of the 11th International Congress on Sound and Vibration*, pages 1–8, 2004.

[19] U. Bolleter, R. Cohen, and J. Wang. Design considerations for an in-duct soundpower measuring system. *Journal of Sound and Vibration*, 28(4):669–685, 1973.

[20] U. Bolleter and M.J. Crocker. Theory and measurement of modal spectra in hard-walled cylindrical ducts. *The Journal of the Acoustical Society of America*, 51:1439, 1972.

[21] BOOST. Users' guides version 4. *Advanced simulation technologies*, 2004.

[22] P.N. Christoffersen, S. Frederiksen, and S.A. Mikkelsen. Progress in SCR denox and silencing technology for diesel engine exhaust systems. In *CIMAC Congress, Copenhagen*, 1998.

[23] J.Y. Chung and D.A. Blaser. Transfer function method of measuring in-duct acoustic properties. I. theory. *The Journal of the Acoustical Society of America*, 68:907–913, 1980.

[24] E. Dokumaci. Sound transmission in narrow pipes with superimposed uniform mean flow and acoustic modelling of automobile catalytic converters. *Journal of Sound and Vibration*, 182(5):799–808, 1995.

[25] E. Dokumaci. On transmission of sound in circular and rectangular narrow pipes with superimposed mean flow. *Journal of Sound and Vibration*, 210(3): 375–389, 1998.

[26] T. Elnady and M. Åbom. SIDLAB: new 1D sound propagation simulation software for complex duct networks. Proceedings of the 13th International Congress on Sound and Vibration , Vienna, Austria, 2006.

[27] T. Elnady, M. Åbom, and S. Allam. Modeling perforates in mufflers using two-ports. *Journal of Vibration and Acoustics*, 132:061010, 2010.

[28] T. Elnady, S. Elsaadany, and M. Åbom. Flow and pressure drop calculation using two-ports. *Journal of Vibration and Acoustics*, 133:041016, 2011.

[29] T. Elnady, S. Elsaadany, and D.W. Herrin. Investigation of the acoustic performance of after treatment devices. *SAE International Journal of Passenger Cars-Mechanical Systems*, 4(2):1068–1075, 2011.

[30] P. Forchheimer. Wasserbewegung durch boden. *Zeitschrift des VDI 50*, 1901.

[31] H. Gijrath and M. Åbom. A matrix formalism for fluid-borne sound in pipe systems. *ASME 5th International Symposium, New Orleans*, 2002.

[32] R. Glav and M. Åbom. A general formalism for analyzing acoustic 2-port networks. *Journal of Sound and Vibration*, 202(5):739–747, 1997.

[33] R. Glav, H. Bodén, and M. Åbom. An acoustic model for automotive catalytic converters. In *Proceedings of Internoise 1988*, volume 88, pages 1261–1266, 1988.

[34] GT-POWER. User's manual version 7.0. *Gamma Technologies*, 2009.

[35] M. Gupta. The Wärtsilä compact silencer system. *Wärtsilä technical journal in detail*, (2):50–54, 2012.

[36] V.H. Gupta and M.L. Munjal. On numerical prediction of the acoustic source characteristics of an engine exhaust system. *The Journal of the Acoustical Society of America*, 92:2716, 1992.

[37] M. Happonen, P. Matilainen, K. Kanniainen, T. Kinnunen, P. Karjalainen, J. Heikkilä, T. Rönkkö, J. Keskinen, T. Lähde, A. Malinen, L. Pirjola, and T. Tzamkiozis. The effect of a particle oxidation catalyst (POC®) on particle emissions of a GDI car during transient engine operation. *SAE Technical Paper 2013-01-0839*, 2013.

[38] R.N. Hota and M.L. Munjal. Approximate empirical expressions for the aeroacoustic source strength level of the exhaust system of compression ignition engines. *International Journal of Aeroacoustics*, 7(3):349–371, 2008.

[39] A. Hynninen and M. Åbom. Procedure to estimate the in-duct sound power in the high frequency range with non-plane waves. *ASME 2012 Noise Control and Acoustics Division Conference at Inter-Noise 2012, New York City, New York, USA*, pages 181–191, 2012.

[40] A. Hynninen and M. Åbom. Acoustic simulation of medium speed IC-engine exhaust gas after treatment devices with substrate. *SAE Technical Paper 2014-01-2057*, 2014.

[41] A. Hynninen and M. Åbom. Acoustic source characterization for prediction of medium speed diesel engine exhaust noise. *Journal of Vibration and Acoustics*, 136:021008, 2014.

[42] A. Hynninen and M. Åbom. Simulation of the particle oxidation catalyst POC® acoustics. *Noise Control Engineering Journal*, 62(5):368–374, 2014.

[43] A. Hynninen and M. Åbom. Determination of in-duct sound power beyond the plane wave range using wall-mounted microphones. *Applied Acoustics*, 99: 24–30, 2015.

[44] A. Hynninen and M. Åbom. Procedure to estimate the acoustic performance of the particle oxidation catalyst POC® with low mach-number flows. *Inter-Noise*, 2015.

[45] A. Hynninen, H. Isomoisio, M. Åbom, and E. Nousiainen. On acoustic performance of the particle oxidation catalyst POC®. Proceedings of Baltic Nordic Acoustic Meeting- BNAM, 2014.

[46] A. Hynninen, R. Turunen, M. Åbom, and H. Bodén. Acoustic source data for medium speed IC-engines. *Journal of Vibration and Acoustics*, 134:051008, 2012.

[47] ISO-10534-1. Acoustics. determination of sound absorption coefficient and impedance in impedances tubes. part 1: Method using standing wave ratio, 2001.

[48] ISO-10534-2. Acoustics, determination of sound abosorption coefficient and impedance in impedance tubes: Part 2, transfer-function method, 1998.

[49] ISO-3740. Acoustics - determination of sound power levels - guidelines for the use of basic standards, 2000.

[50] ISO-3741. Acoustics - determination of sound power levels and sound energy levels of noise sources using sound pressure - precision methods for reverberation test rooms, 2010.

[51] ISO-5136. Acoustics - determination of sound power radiated into a duct by fans and other air-moving devices - in-duct method, 2009.

[52] ISO-7235. Acoustics - laboratory measurement procedures for ducted silencers and air-terminal units - insertion loss, flow noise and total pressure loss, 2003.

[53] C.-G. Johansson, K. Saine, P. Johansson, and M. Åbom. Exhaust noise - a new novel in situ measurement technology in duct. *Proceedings of the 12th International Congress on Sound and Vibration*, 2005.

[54] P. Joseph, C.L. Morfey, and C.R. Lowis. Multi-mode sound transmission in ducts with flow. *Journal of Sound and Vibration*, 264(3):523–544, 2003.

[55] J. Jurkiewicz, A. Snakowska, and D. Smolik. Acoustic impedance of outlet of a hard-walled unbaffled cylindrical duct for multimode incident wave. *Acta Physica Polonica A, Acoustic and Biomedical Engineering*, 119(6-A):1061–1067, 2011.

[56] D.H. Keefe. Acoustical wave propagation in cylindrical ducts: Transmission line parameter approximations for isothermal and nonisothermal boundary conditions. *The Journal of the Acoustical Society of America*, 75(1):58–62, 1984.

[57] T Kinnunen, P Matilainen, D Scheder, W Czika, D Waters, and G Russ. Particle oxidation catalyst (POC®)-from diesel to gdi-studies on particulate number and mass efficiency. *SAE Technical Paper 2012-01-0845*, 2012.

[58] M. Knutsson. *Modelling of IC-Engine Intake Noise*. PhD thesis, The Marcus Wallenberg Laboratory for Sound and Vibration Research, Royal Institute of Technology, Stockholm, Sweden, 2009.

[59] J. Lavrentjev and H. Tiikoja. Investigation of wave propagation and radiation in ducts with arbitrary environment by using the three-microphone method. *Internoise*, 2008.

[60] K. Lehtoranta, P. Matilainen, J. Åsenbrygg, A. Lievonen, T. Kinnunen, J. Keskinen, and A. Solla. Particle oxidation catalyst in light duty and heavy duty diesel applications. *SAE Technical Paper 2007-24-0093*, 2007.

[61] K. Lehtoranta, P. Matilainen, T. Kinnunen, J. Heikkilä, T. Rönkkö, J. Keskinen, and T. Murtonen. Diesel particle emission reduction by a particle oxidation catalyst. *SAE Technical Paper 2009-01-2705*, 2009.

[62] A. Michalke. On the propagation of sound generated in a pipe of circular cross-section with uniform mean flow. *Journal of Sound and Vibration*, 134 (2):203–234, 1989.

[63] A. Michalke. On experimental sound power determination in a circular pipe with uniform mean flow. *Journal of Sound and Vibration*, 142(2):311–341, 1990.

[64] C.L. Morfey. Acoustic energy in non-uniform flows. *Journal of Sound and Vibration*, 14(2):159–170, 1971.

[65] M. L. Munjal. *Acoustics of Ducts and Mufflers with Application to Exhaust and Ventilation System Design*. John Wiley & Sons, New York, 1987.

[66] M. L. Munjal. Acoustic characterization of an engine exhaust source - a review. *Proceedings of Acoustics 2004*, 2004.

[67] W. Neise and F. Arnold. On sound power determination in flow ducts. *Journal of Sound and Vibration*, 244(3):481–503, 2001.

[68] K.S. Peat. A first aproximation to the effects of mean flow on sound propagation through cylindrical capillary tubes. *Journal of Sound and Vibration*, 175 (4):475–489, 1994.

[69] K.S. Peat. Convected acoustic wave motion along a capillary duct with an axial temperature gradient. *Journal of Sound and Vibration*, 203(5):855–866, 1997.

[70] K.S. Peat and R. Kirby. Acoustic wave motion along a narrow cylindrical duct in the presence of an axial mean flow and temperature gradient. *The Journal of the Acoustical Society of America*, 107:1859, 2000.

[71] A.D. Pierce. *Acoustics: an introduction to its physical principles and applications*. Acoustical Society of America, 1989.

[72] E. Rubiola and F. Vernotte. The cross-spectrum experimental method. *arXiv preprint arXiv:1003.0113*, 2010.

[73] A. Saarinen and S. Uosukainen. Jmc-method experiences of sound attenuation in ventilation duct. Proceedings of Euronoise 2006, 2006.

[74] M.P. Sacks, J.G. Kawall, R. Behboudi, and J. Buttell. In-duct measurement of gas turbine noise emissions using a cross spectrum method. *ASME turbo show, Munich*, 2000.

[75] A. Selamet, V. Easwaran, JM Novak, and RA Kach. Wave attenuation in catalytic converters: reactive versus dissipative effects. *The Journal of the Acoustical Society of America*, 103(2):935–943, 1998.

[76] N. Soikkeli, M. Lehikoinen, and K.-O. Rönnback. Design aspects of SCR systems for HFO fired marine diesel engines. Proceedings of the CIMAC Congress, Shanghai, 2013.

[77] M.R. Stinson. The propagation of plane sound waves in narrow and wide circular tubes, and generalization to uniform tubes of arbitrary cross-sectional shape. *The Journal of the Acoustical Society of America*, 89:550, 1991.

[78] WAVE. User's manual version 8.0. *Ricardo*, 2013.

[79] D.E. Winterbone and R.J. Pearson. *Design Techniques for Engine Manifolds, Wave Action Methods for IC-engines*. Professional Engineering Publishing, 1999.

[80] D.E. Winterbone and R.J. Pearson. *Theory of Engine Manifold Design, Wave Action Methods for IC-engines*. Professional Engineering Publishing, 2000.

[81] C. Zwikker and C.W. Kosten. Sound absorption materials. 1949.

Part II

Appended papers